Scientia Marina 85(4)
December 2021, 225-244, Barcelona (Spain)
ISSN-L: 0214-8358
https://doi.org/10.3989/scimar.05110.020

Geochronology and palaeoclimatic context of submerged siliciclastic beachrock formation in the western Mediterranean Sea

Carles Roqué Pau [1], Mario Zarroca Hernández [2], Rogelio Linares Santiago [2]

[1] Àrea de Geodinàmica Externa i Geomorfologia, Universitat de Girona, E-17003 Girona, Spain.
(CRP) (Corresponding author) E-mail: carles.roque@udg.edu. ORCID iD: https://orcid.org/000-0003-0650-160X
[2] Geology Department, Universitat Autònoma de Barcelona, E-08193-Bellaterra, Barcelona, Spain.
(MZH) E-mail: mario.zarroca.hernandez@uab.cat. ORCID iD: https://orcid.org/000-0001-6907-1892
(RLS) E-mail: Rogelio.Linares@uab.cat.

Summary: This article describes the geomorphological and petrological characteristics of 19 submerged beachrocks located on the north Catalan coast (western Mediterranean Sea). Their length ranges between 8 and 1039 m, their width between 1.5 and 86.5 m and their thickness between 0.4 and 3.25 m. They are siliciclastic beachrocks consisting of well-rounded gravels with a very coarse sand matrix, and they have a low proportion of bioclasts (<1%). Cementation occurred in the swash zone and adjacent foreshore due to the precipitation of high magnesium calcite. From absolute dates (^{14}C and optically stimulated luminescence) and anthropic artifacts, three phases of formation attributable to the Late Holocene were identified. Phase I corresponds to the warm and humid Roman Period and was recorded at a level below -3.75 m mean sea level (MSL). Phase II corresponds to the warm and arid Medieval Climate Anomaly and was recorded at +0.25 m to -2.5 m MSL. Phase III corresponds to the Little Ice Age and Industrial Period and was recorded at levels ranging from +0.5 m to -3.0 m MSL. Good temporal correspondence between the chronology of the cementation phases and warm and/or dry palaeoclimatic conditions can be established.

Keywords: late Holocene; beach deposits; ^{14}C; optically stimulated luminescence; archaeological remains.

Contexto geocronológico y paleoclimático de la formación de playas fósiles sumergidas en el Mediterráneo Occidental

Resumen: En este artículo se describen las características geomorfológicas y petrológicas de 19 playas fósiles sumergidas localizadas en la costa norte catalana (Mediterráneo Occidental). Su longitud oscila entre 1039 m y 8 m, y su anchura entre 86.5 m y 1.5 m. Su espesor varía entre un mínimo de 0.4 m y un máximo de 3.25 m. Se trata de playas fósiles siliciclásticas, constituidas por gravas bien redondeadas, con matriz de arena muy gruesa. Presentan una baja proporción de bioclastos (<1%). La cementación se produjo en la zona de batida de la playa debido a la precipitación de calcita magnesiana. A partir de dataciones absolutas (^{14}C y OSL) y de artefactos antrópicos, se han identificado tres fases de formación atribuibles al Holoceno superior. La fase I corresponde al periodo cálido y húmedo romano, y ha sido registrada en un nivel situado por debajo de los –3.75 m respecto del nivel medio del mar (MSL). La fase II encaja con la anomalía climática cálida y árida medieval, la cual ha sido registrada entre +0.25 m y –2.5 m MSL. La fase III corresponde a la pequeña edad del hielo y al periodo industrial, y ha sido registrada en niveles situados entre +0.5 m y –3.0 m MSL. Se puede establecer una buena correspondencia temporal entre la cronología de las distintas fases de cementación y las condiciones paleoclimáticas cálidas y/o áridas.

Palabras clave: Holoceno superior; depósitos de playa; ^{14}C; OSL; restos arqueológicos.

Citation/Como citar este artículo: Roqué Pau C., Zarroca Hernández M., Linares Santiago R. 2021. Geochronology and palaeoclimatic context of submerged siliciclastic beachrock formation in the western Mediterranean Sea. Sci. Mar. 85(4): 225-244. https://doi.org/10.3989/scimar.05110.020

Editor: P. Puig.

Received: August 3, 2020. **Accepted:** July 12, 2021. **Published:** November 18, 2021.

INTRODUCTION

Beachrocks are consolidated coastal deposits formed by the lithification of beach sediments due to the precipitation of calcium carbonate (mostly high magnesium calcite and/or aragonite, but also low magnesium calcite) (e.g. Scoffin and Stoddart 1987, Psomiadis et al. 2009). Typically, cementing occurs in the intertidal zone and under a thin layer of unconsolidated sediments (Webb et al. 1999), although cementing in the supratidal zone has also been reported (Kelletat 2006). Beachrocks are formed both on beaches with a predominance of carbonaceous and siliciclastic particles and on beaches with silt to cobble-size sediments (Moissette et al. 2013). Cementation is a very rapid process at a geological time scale, being of the order of months to years (Hopley 1986), so the granulometric and compositional characteristics of the beachrock reflect those of the beach from which they are formed (Psomiadis et al. 2014). Artifacts of human origin, such as fragments of ceramic, glass and metal objects have also been documented to be embedded in beachrocks (Gischler 1994, Friedman 1998, Pullen 2013). The specific physico-chemical and/or biological processes involved in carbonate precipitation at the earliest genetic stages have given rise to controversy and a disparity of models. A good synthesis of these is included in the works of Turner (2005) and Danjo and Kawasaki (2014). The main primary cementing mechanisms proposed are physicochemical, linked to (1) the common ion effect in the mixture of meteoric and sea water, (2) evaporation and (3) degassing of CO_2. Recent studies show that carbonate precipitation induced by the activity of microorganisms plays an important role in the cementation of beachrocks (McCutcheon et al. 2016, 2017, Ramachandran et al. 2020, Daryono et al. 2020).

Beachrocks form laminar ledges oriented parallel to the beach and can reach a few kilometres in length and up to several hundred metres in width. They are relatively thin, and generally ranging from 0.3 m to 3 m (Vieira and Ros 2006, Vousdoukas et al. 2009). Usually they do not fully cover the entire length of the beach but emerge forming isolated outcrops of cemented sediments limited by unconsolidated sediments (Kelletat 2006). Most of the described beachrocks lie on unconsolidated beach deposits, but they can also lie directly on rocky substrates (Turner 2005). They are constructed by a sequence of layers ranging from 5 to 30 cm thickness, tilted 5º to 15º towards the offshore (Font and Calvet 1997, Calvet et al. 2003).

Pleistocene and even older beachrocks have been reported (e.g. Yaltirak et al. 2002). However, their age of formation, based on the dates reported in the literature, range mostly between 5000 and 1000 yr BP (Vousdoukas et al. 2007, Danjo and Kawasaki 2014). Flandrian beachrocks are considered good geoindicators of the position of the sea level and are therefore useful for the reconstruction of palaeoshorelines and for establishing sea level oscillation throughout the Holocene (Caldas et al. 2006, Stattegger et al. 2013, Mauz et al. 2015, Vacchi et al. 2016). Recently constructed beachrocks are usually partially buried under emerged sediments from the active beaches (Russell and McIntire 1965, Neumeier 1998). Neotectonics and isostatic adjustment can make the position of beachrocks vary significantly on a scale of decades or centuries (e.g. Avcioglu et al. 2016, Erginal et al. 2021), but in the absence of neotectonics their position is determined by the coastal dynamics. Thus, on prograding coasts, beachrocks are abandoned behind the active beach, while on retrograding coasts they are exposed to the open sea and end up totally or partially submerged (Turner 2005). Long-term uplift and subsidence determine the beachrocks' position. They form alignments parallel to the beach located at different heights, both below and above sea level (Mouslopoulou et al. 2015). In submerged sequences, beachrocks tend to be progressively older at greater depth and at greater distance from the coast (Strasser et al. 1989, Neumeier 1998).

Beachrocks are mostly located in tropical and sub-tropical regions. The majority (90%) are distributed between the Tropic of Capricorn and the 40ºN parallel, with little presence around the Ecuador (Danjo and Kawasaki 2014). Modern beachrocks are restricted to warm climates, specifically between latitudes 35ºN and 35ºS (Friedman 2011). This distribution seems to indicate that sea surface temperature is a key controlling factor in their build-up. However, a few examples of beach sediments cemented by calcium carbonate have also been reported in temperate-humid regions (Kneale and Viles 2000, Rey et al. 2004, Arrieta et al. 2011). Quaternary variations in local climatic conditions may explain the presence of beachrocks in relatively cool regions, so it is essential to accurately establish the chronology of the cementation processes.

Pleistocene and Holocene beachrocks are frequent in the Mediterranean Sea, especially in the eastern sector. They have been described on the Aegean coast (e.g. Moissette et al. 2013, Psomiadis et al. 2014, Mouslopoulou et al. 2015) and on the coasts of Egypt (El-Sayed 1988, Holail and Rashed 1992), Israel (Magaritz et al. 1979) and Tunisia (Strasser et al. 1989). Their arrangement in the western Mediterranean is much less known, although they have been described on the coasts of Liguria (Bloch and Trichet 1966), Corsica (Bernier et al. 1997), Balearic Islands (Muhs et al. 2015) and Barcelona (Russell 1962, Vousdoukas et al. 2007).

Here we describe a set of beachrocks located on the Costa Brava, on the northern part of the Catalan coast (western Mediterranean Sea). They are submerged deposits with a predominance of siliciclastic particles. There is little previous literature reporting on these beachrock deposits. Roqué and Pallí (1995, 1997) describe the existence of two formation phases, based on geomorphological criteria, the presence of archaeological artifacts encased in the deposits, and a single ^{14}C dating (not calibrated). These two recognized phases are linked to (a) beachrocks located between +0.25 m and -2.5 m MSL, dating from 1950 to 1800 yr BP, and (b) beachrocks located between -2 m and -4 m MSL, attributed to the Holocene.

The specific aims of this study were (1) to further analyse the geomorphological and petrological features of these deposits; (2) to accurately establish the chro-

nology of the cementation episodes by means of absolute dating (^{14}C and optically stimulated luminescence (OSL)) and relative dating (archaeological remains); and (3) to observe possible relationships between the geochronology of the formation episodes and the prevailing palaeoclimatic conditions, in order to establish whether their genesis is controlled by climatic factors.

STUDY AREA

The study area comprises *ca*. 215 km of the Costa Brava, on the northern part of the Catalan coast, NE Iberian Peninsula (western Mediterranean). It is a mostly rocky coast that extends from the Tordera River delta in the south to the Pyrenees mountain range in the north (Fig. 1). Three deltaic systems (the Tordera, Ter and Fluvià-Muga) occupy 29.1 km of the total coast, and the rest corresponds to a rocky coast with cliffs and small beaches in coves (Calvet and Gallart 1973, Casas-Prat and Sierra 2012, Furlani et al. 2014). The deltas separate the rocky coast into three sectors with different geological features: (1) the South Sector, 90.0 km long, with a predominance of Palaeozoic granitic rocks, (2) the Central Sector, 20.4 km long, formed by Mesozoic limestones, and (3) the North Sector, 75.2 km long, with a predominance of Palaeozoic schist.

The climate of the study area is Mediterranean. Average annual rainfall varies between 480 and 700 mm. The mean annual air temperature ranges from 15°C to 16°C, with a minimum monthly average of 8°C to 9°C (January) and a maximum monthly average of 22°C to 23°C (July) (Martín-Vide and Raso 2008). The mean annual sea surface temperature (SST) is 17.1°C, with a minimum monthly average of 12.6°C (February) and a maximum monthly average of 22.9°C (August) (data from the Catalan Meteorological Service for the period 2000-2015, corresponding to the observation point in L'Estartit [42°03'N, 3°15'E] located 1.8 km offshore of the Medes Islands). Mean annual SST in the study area increases from north to south by 0.55±0.05ºC per 100 km (Serrano et al. 2013). According to Serrano et al. (2013), the average annual SST for the period 2003-2010 was 16.7°C in Port de la Selva, 16.9°C in Cadaqués, 17.0°C in the Medes Islands and 17.4°C in Port d'Aro (see locations in Fig. 1).

The astronomic tidal range is of about 15 cm in the area (Sanuy et al. 2020). The available data on the annual sea level variation recorded in the L'Estartit harbour show a maximum oscillation of +25 cm to –15 cm, which is linked to the variation of atmospheric pressure (data for 2017 according Pascual [2019]). Wave climate along the Costa Brava is characterized by wave calms from May to September and energetic storms from October to April, with an average duration of less than 24 h (Mendoza et al. 2011). The directional distribution of winds produces a predominance of waves coming from the NW and N in the northern part of the study area and from the E and S in the southern part. The largest waves come from the E or E-NE, where the largest fetches (up to 600 km) and strongest winds coincide (Sánchez-Arcilla et al. 2008, Casas-Prat and Sierra 2012). The average frequency of storms is five per year (Gómez et al. 2005, Sánchez-Arcilla et al. 2008). Severe and extreme intensity storms reach wave heights (Hs) of the order of 5.1 to 6.6 m, with average return periods of *ca*. 10 and 50 yr, respectively (Mendoza et al. 2011).

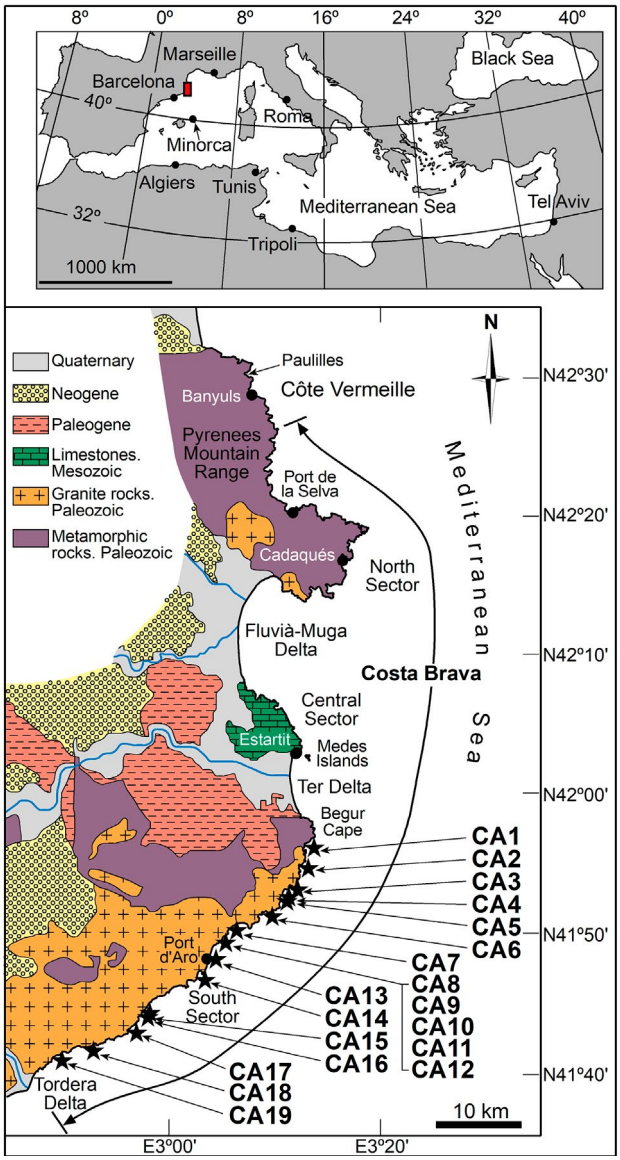

Fig. 1. – Location and geological setting of the study area. Beachrocks: CA1, Platja Fonda. CA2, Tamariu. CA3, Llafranc. CA4, Canadell. CA5, Port Pelegrí. CA6, Cap Planes. CA7, St Antoni. CA8, Paller. CA9, Puget. CA10, Roig. CA11, Belladona. CA12, Pi. CA13, Platja Aro. CA14, St Pol. CA15, Futadera. CA16, Giverola. CA17, Mar Menuda. CA18, Canyelles. CA19, Fenals.

METHODOLOGY

Beachrock location and description

An exhaustive inventory of beachrocks was carried out by means of an extensive photogeological survey of the coast, encompassing the analysis of the available vertical aerial orthoimage series from different years (1946, 1956, 1986, 1991, 1994, 1996, 2000, 2001, 2002, 2004, 2006 and 2008 to 2018) at different resolu-

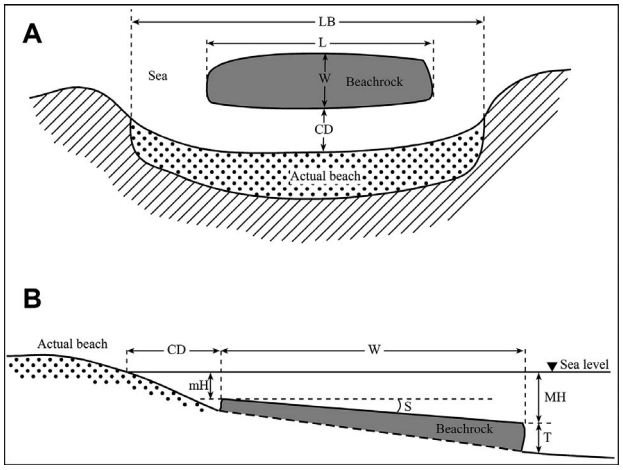

Fig. 2. – Main morphometric features of beachrocks. A, plan view: LB, length of the current beach. L, beachrock length. W, beachrock width. CD, coastal distance. B, cross section: CD, coastal distance. W, beachrock width. mH, minimum depth. MH, maximum depth. T, thickness. S, slope.

tions (100 to 25 cm/px) and different spatial coverages (data from the Catalan Cartographic and Geological Institute (ICGC) (www.icc.cat/vissir3/) and Google Earth Pro servers). Regarding the identification of seabed morphological features, the image resolution is limited by (1) the absolute resolution of the image, (2) the sea condition at the collecting time, (3) the angle of light-incidence, and (4) the shadows cast by the coastal cliffs. In optimal conditions, beachrocks are clearly identified down to –10 m MSL.

Georeferenced images and the ICGC viewer were used to measure the length (L) and the width (W) of the exposed deposits and their minimum distance from the shoreline (the coastal distance) (Fig. 2). The coastal distance was measured according to the criteria of Pagán et al. (2016), which take as a reference the run-up limit or boundary of the wet beach in the orthoimages.

The inventoried beachrocks were studied in situ during diving surveys from 2009 to 2020; the observations performed during the dives carried out in 1995 and 1996 were also revised and updated. The visible thickness (T) was measured in exposed sections by means of a 1-metre scale (10 cm divisions). The minimum (mH) and maximum (MH) depth of shallow deposits were measured with the 1-metre scale. A plumb bob was used to measure the deepest ones. The sea level at the time of diving was taken as a reference. A ±0.25 m systematic error was assumed because of the maximum sea level variation over the year. The slope of the beachrock surface (S) was estimated as the gradient between the variation of depth and the distance along a transect perpendicular to the maximum slope (Fig. 2). The dimensions (L and W) were verified by positioning the limits using GPS integrated in Olympus TG5 and TG6 underwater cameras. The attitude of plains (joints, layers, etc.) was measured by means of the digital compass fitted in these cameras. The erosional landforms, internal layers and the features of the underlying substrate were also measured, described and photographed.

Petrology characterization

During the diving surveys, 30-cm-long rock block samples were extracted for petrological and textural characterization of the deposits by means of mace and chisel. Beachrocks are usually colonized on their surface by calcareous fouling organisms (e.g. Rhodophyta, Bryozoa and molluscs), so the external part of the block samples was removed by a diamond disc grinder. The resulting fresh blocks were conditioned to extract petrographic thin sections for microscope analysis. The study of the sediments was complemented with direct observation of the blocks with a binocular magnifying glass (×10 to ×100). The percent weight content of carbonates was roughly determined by dissolving 250 g of dry sample in HCl and comparing the initial and final weights.

Mineralogical analysis of 12 selected samples was performed by X-ray powder diffraction (XRD) (Bruker AXS D8 Advance Powder RX Diffractometer from the University of Girona Technical Research Services (STRUdG)) to determine the composition of the carbonate cement. A ZEISS DSM-960A scanning electron microscope (SEM) equipped with an Oxford Link Isis L200B energy separation RX (EDX) detector from the STRUdG was used to photograph and determine the elemental composition of the 12 samples.

Sediments of the beaches adjacent to the beachrocks were also sampled for textural and compositional analysis. A total of 1 kg of sediment was collected in three separate sampling stations at *ca*. +1.0 m and –1.5 m MSL (foreshore and upper shoreface, respectively, e.g. Longhitano (2015)). Particle size distribution was obtained with a standard nested column of sieves and a mechanical shaker. The petrological composition of the sediment was determined from the identification of a minimum of 250 grains using a binocular magnifying glass (×10 to ×100).

Dating methods

A total of 12 carbonate shells of marine molluscs (7 gastropods and 5 bivalves) included in 7 of the beachrocks (CA1, 3, 6, 7, 11, 14 and 17) were dated by the ^{14}C method. A 30-cm-thick sample of a red algae crust embedded in CA14 and a charcoal fragment included in CA17 were also dated.

^{14}C ages were measured in the laboratories of the Tritium and ^{14}C Dating Service of the Universitat Autònoma de Barcelona, the Poznan Radiocarbon Laboratory and Beta Analytic.

The content of carbonate seashells of size greater than 2 mm in the collected samples ranged only from 0.004 g kg^{-1} to 0.4 g kg^{-1}, which posed a severe constraint for ^{14}C dating. However, in the beachrocks located at depths of less than –2 m MSL, some relatively large shells were recovered directly during the diving observations. Only samples lying on eroded clean surfaces and lacking coating of living organisms were

collected (i.e. CA1, 2, 3, 11, 14 and 18). Where large shells were not available, it was attempted to extract large bioclasts from rock block samples according to the following procedure: (1) the external portion of the blocks was removed by a diamond disc grinder; (2) the clean block was crushed by means of a hammer to obtain fragments of *ca*. 1 to 5 mm in diameter; (3) finally, the bioclasts were selected using a binocular magnifying glass. This allowed us to obtain additional dateable material from CA6, 7 and 17. However, as explained below, not all recovered bioclasts were considered appropriate for dating.

The seashells provide a *terminus post quem* age for the beach cementation. To minimize the age difference between the death of seashell animals and the time of cementation of the beach, the bioclasts for dating were selected according to the following criteria: (1) skeletons of perforating organisms were discarded because, although they are located inside the block, they may postdate the deposit; and (2) because the post mortem residence time of the seashells on the beaches is a priori uncertain, shells were selected preferably without fragmentation and little erosion or bioerosion in order to avoid dating bioclasts that could have been sedimented on the beach long time before the cementation. Due to these criteria, several broken, eroded and burrowed seashells (mostly of *Spondylus gaederopus*) recovered from CA1, 2, 3, 11, 14 and 18 were dismissed for dating.

Conventional ^{14}C ages were converted to calendar ages using the CALIB 8.2 programme (Stuiver et al. 2021) and were adjusted to two standard deviations (2σ). The Marine 20 dataset was used to calibrate the samples that corresponded to sea-living organisms. In these cases, calibration must also consider the marine reservoir effect, which makes the radiometric ages older than the contemporary ones under atmospheric conditions. However, there is significant bias due to the local marine conditions (ΔR). Here, a ΔR value of –140±74 yr was used, according to the mean values of the eight nearest (<400 km) points from the study area in which the ΔR value was reported (Siani et al. 2000). This ΔR value was contrasted by comparing the calibrated ages obtained for a seashell and for charcoals included in the same rock block sample of CA17. Both the charcoal and the shell were expected to be the same age.

Absolute ^{14}C dating was complemented with two OSL dates of quartz grains included in the CA3 and 14 beachrocks. OSL dates were measured in the Luminescence Dating Laboratory of the University of A Coruña. One of the blocks dated by OSL corresponded to the same rock block sample from which a seashell was dated by ^{14}C (i.e. CA3). The OSL age corresponded to the time of burial of the quartz grains, so it cannot be earlier than the age of the seashell. Both ages (OSL and ^{14}C) obtained for the same rock block sample also allowed us to establish the extent to which the ΔR value used in the ^{14}C calibration was correct.

The absolute dating was complemented by the age analysis of pottery remains embedded in CA3, 4, 7, 14 and 18. This allowed us to establish a relative *terminus post quem* age for the cementation of the deposits. These materials were recovered directly by diving visual reconnaissance of surfaces free of algae and encrusting organisms. The Archaeology Laboratory of the University of Girona and the Terracotta Museum (La Bisbal d'Empordà) supported us in classifying and establishing their chronological rank.

RESULTS

Beachrock inventory and spatial distribution

Up to 19 beachrocks were documented along the 215 km of the studied coastline, all of them submerged (Fig. 1). Six of them form sequences of two or more partially overlapped ledges. Their spatial distribution is highly irregular, because all the beachrocks are concentrated in the south sector of the Costa Brava. Neither the aerial photography analysis nor the diving surveys revealed any beachrock in the central and northern sectors. Fifteen kilometres north of the Costa Brava's northernmost boundary, we found the only beachrock that we identified and explored, on Paulilles on the Côte Vermeille beach (Fig. 1).

The analysis of the temporal series of orthoimages from consecutive years revealed that some beachrocks had been exhumed by the intense wave erosion during the rough storms events of December 2008 and January 2017 and had subsequently been partially or totally buried. This analysis was not possible for the previous severe and extreme storms catalogued by Mendoza et al. (2011) and Sanuy et al. (2020) (i.e. November 1982, February 1996, December 1997, December 2000, November 2001, December 2001 and October 2003), because the orthoimages older than 2008 are not consecutive or do not cover the entire study area. During the storm in December 2008, one of the most severe recorded on this coast since 1984 (Mendoza et al. 2011, Sanchez-Vidal et al. 2012), CA13 and 19 were exposed for the first time. Furthermore, CA2, 4, 7, 9 and 14 increased in length and/or width. The effects of the January 2017 storm were especially noticeable on CA13 and 14, which were once again much more exposed. The Gloria Storm of January 2020 (which is younger than the time period analysed by orthoimages) exhumed CA5, of which there was no documentary or oral record to date. Therefore, our inventory could not be considered exhaustive, because there must be additional buried beachrocks in the study area that have not emerged but remain hidden under a sediment cover.

Morphological characteristics

The morphometric parameters of the beachrocks are shown in Table 1. Length and width data correspond to the maximum values measured in the analysed orthoimages (from 1946 to 2018) and diving surveys (from 2009 to 2020). A single deposit unit was considered if more than one isolated deposit was in the same cove. It should be noted that the current CA3 and CA7 beaches have been subject to nourishment and sand transfer works in the last four decades, so length and weight values of these submerged deposits are influenced by the presence of artificially driven sediments.

Fig. 3. – Examples of beachrocks. A, vertical view of CA15 beachrocks ledges (a-e) (yellow dot lines) and the current beach (red dot line). B, view of the CA1 beachrock ledges a and b (yellow dot lines); ledge b eastern part is degraded (at the bottom of the image). C, inner layers (upper level of CA14 beachrock). D, partially emerged beachrock (CA11).

Table 1. – Morphometric characteristics of the beachrocks: length (L) and width (W) (maximum measured values); depth (D) (negative values refer to depth below MSL); thickness (T); number of differentiated ledges (sequences) of beachrock (seq. num.); base (substratum at the base of beachrock: R=rock; UBS=unconsolidated beach sediments); slope towards the open sea (S); length of the current beach on which the beachrock is located (LB); beachrock length/width ratio (L/LB); coastal distance (CD) is the minimum distance between shoreline and outcropping beachrock.

Code	Location	L (m) ±0.5	W (m) ±0.5	mH/MH (m) ±0.25	T (m) ±0.25	Seq num	Base	S (°) ±1°	LB (m) ±0.5	L/W	L/LB	CD (m) ±0.5
CA1	Platja Fonda	132.5	32.0	-1.0 / -5.0	1.25	2	R	5	165	4.14	0.80	1.0
CA2	Tamariu	8.0	1.5	-0.5 / -1.0	0.4	1	R	5	196	5.33	0.04	0.5
CA3	Llafranc	75.0	14.0	-1.0 / -3.0	2.0	1	R	5	324	5.36	0.23	5.5
CA4	Canadell	8.0	1.5	-0.25 / -1.0	0.5	1	R	5	185	5.33	0.04	3.0
CA5	Port Pelegrí	53.0	4.5	-0.25 / -2.5	0.5	1	R	5	58	11.77	0.91	1.0
CA6	Cap Planes	287.0	73.0	+0.25 / -4.5	1.5	6	R	7	478	3.93	0.60	0.0
CA7	St Antoni	1039.0	27.0	-1.0 / -4.0	2.25	1	R-UBS	5	3434	38.48	0.30	12.5
CA8	Paller	21.5	9.5	-0.5 / -2.0	1.0	1	R	5	30	2.26	0.72	4.5
CA9	Puget	148.0	12.5	-1.0 / -2.5	1.25	1	R	5	456	11.84	0.32	9.5
CA10	Roig	60.0	9.5	-0.25 / -2.0	1.5	1	R	5	109	6.32	0.55	3.5
CA11	Belladona	81.0	18.5	+0.5 / -2.0	1.5	1	R	5	89	4.38	0.91	0.0
CA12	Pi	35.0	9.5	-0.5/ -2.0	1.0	1	R	4	41	3.68	0.85	2.0
CA13	Platja Aro	524.0	8.0	-1.0 / -2.5	>1.5	1	UBS?	5	2110	65.50	0.25	10.5
CA14	St Pol	619.0	19.5	-0.25 / -2.5	>2.0	2	UBS?	8	842	31.74	0.74	3.0
CA15	Futadera	264.0	86.5	-0.5 / -4.0	2.0	5	R	8	81	3.05	3.26	1.0
CA16	Giverola	73.0	34.0	-0.5 / -2.5	2.0	2	R	8	167	2.15	0.44	1.0
CA17	Mar Menuda	132.5	27.0	-2.0 / -5.25	3.25	2	R	5	745	4.91	0.18	12.5
CA18	Canyelles	58.0	7.5	-0.5 / -2.0	1.5	1	R	5	467	7.73	0.12	4.5
CA19	Fenals	132.0	12.5	-0.5 / -2.5	>1.0	1	R?	5	717	10.56	0.18	12.0

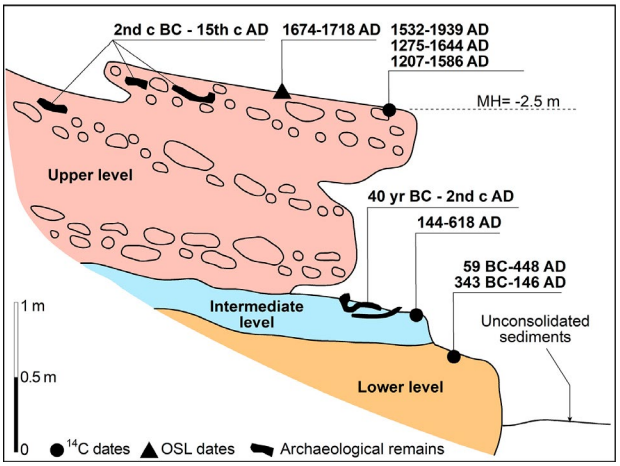

Fig. 4. – Schematic cross section and chronology of the CA14 (St Pol) beachrock. The upper level is constructed by cemented very fine to fine gravels with sparse very coarse clasts, and includes pottery remains. The intermediate level is a coralline algae calcareous bed, also with pottery remains. The lower level is built up of coarse to very coarse sand with sparse fine gravel clasts.

Length varies between a 8 and of 1039 m. CA7 (1039 m), CA14 (619 m) and CA13 (524 m) were the longest and CA2 (8 m), CA4 (8 m) and CA8 (21.5 m) were the shortest. The ratio between beachrock length and the length of the beaches on which they are located was variable and usually less than 1. This is in accordance with the fact that the degree of cementation was variable, causing the beachrocks to be only partially formed or preserved (e.g. Kelletat 2006). However, CA15 exceeded the current beach length by 3.26 times, which indicates a greater deposit development at the time of its cementation (Fig. 3A). Beachrock width also showed a pronounced variability, ranging between 1.5 m (CA2 and 4) and 86.6 m (CA15). This variation was partly caused by the sequence overlapping of two to six contacting ledges, which increased the total width of the deposits. As an example, CA6 (W=73.0 m) was composed of a sequence of six ledges; CA15 (W=86.5 m) was composed of 5 (Fig. 3A); and CA16 (W=34.0 m) and CA1 (W=32.0 m) was composed of 2 (Fig. 3B). The width of those beachrocks formed by a single ledge averaged 10.4 m. Similarly, the mean width of the single ledges that form the wider beachrocks was 11.6 m.

The beachrocks' internal architecture was built up of 5- to 20-cm-thick layers tilted 10° to 12° towards the open sea (Fig. 3C). Their tops were also tilted towards the open sea, averaging values of 4° to 8°, which are lower than those of the lamination. Minimum beachrock top depths (mH) were close to the current sea level; only CA11 (Fig. 3D) and CA6 were partially emerged (+0.5 m and +0.25 m MSL, respectively). Maximum beachrock top depths (MH) ranged between –1 m (CA2 and 4) and –5.25 m MSL (CA17). The deepest levels corresponded to the distal outcrops of the overlapping sequences, as in the case of CA1 (Fig. 3B), CA6, CA15 (Fig. 3A) and CA17. CA7, formed by a single ledge, reaches up to –4.0 m MSL. This is due to the partial deposit collapse caused by the erosion of the subjacent unconsolidated marine sediments. However, the eastern sector of this beachrock lies on a bedrock formed by weathered granite, which is Palaeozoic in age. CA2, 3, 4, 5, 6, 8, 9, 10, 11, 12, 15, 16, 17 and 18 were also placed directly on this same bedrock type. CA1 lay on Palaeozoic granite and schist. No data are available on materials just below CA13, 14 and 19.

Cemented deposit thickness (T) varied between 0.4 m (CA2) and 3.25 m (CA17), averaging 1.5 m. The greater thickness of the beachrock in CA17 is related to the fact that it is built of two partially overlapping ledges. Similarly, in CA14 an upper level of 1.25 m thickness overlaps a lower one, of which a thickness of 0.5 m thick is visible. Both are divided by a 0.3-m-thick bioconstructed calcareous layer of coralline algae embedded above the lower level (Fig. 4).

The minimum distance between the beachrocks and the current beach was generally less than 5 m. Larg-

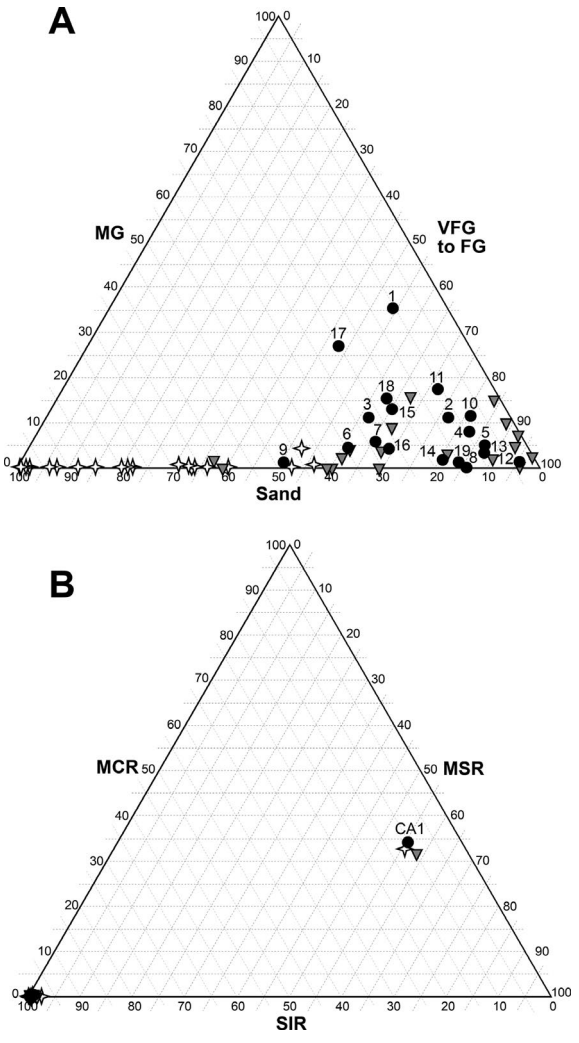

Fig. 5. – A, relative percentage of grain size distribution of beachrock (black circles), foreshore (grey triangles) and upper shoreface (white stars) samples. Numbers correspond to each studied beachrock. MG, medium gravel; VFG, very fine gravel; FG, fine gravel. B, relative percentage of petrological composition of beachrock (black circles), foreshore (grey triangles) and upper shoreface (white stars) samples. SIR, siliceous igneous rocks; SMR, siliceous metamorphic rocks; CMR, calcareous metamorphic rocks.

er distances were recorded on beaches that showed a marked erosive trend in recent decades due to (1) sporadic rough storm effects, as in CA9 (9.5 m), CA13 (10.5 m) and CA19 (12.0 m); (2) generalized sand beach loss, as in CA7 (12.5 m), which led to the installation of rock groynes to counteract the erosion of the sandy coast in the 1970s; and (3) focused erosion caused by the local effect of a small pier that has limited the natural contributions of sediment in CA3 (5.5 m) since 1970.

Petrological characteristics

The petrological characteristics of the studied beachrocks are summarized in Table 2. Overall, the beachrocks are conglomerates of well-rounded gravels with a very coarse sand matrix. Their granulometry ranges between very fine gravel and medium gravel (2 mm to 16 mm) (Figs 5, 6A). The deposits are somewhat graded, with the coarser particles tending to be concentrated towards their base and in the distal part. In CA1, 6 and 15, the ledges furthest from the coastline (and deepest) are composed of larger particles, between medium gravel and cobble, including boulders (>256 mm) at the base of the distal part (Fig. 6B).

The grain size of the sediment from the beaches differs from that of the beachrocks (Table 3, Fig. 5). The particle size of the beachrocks is greater than that of the samples collected on the beaches at -1.5 m MSL (upper shoreface), in which sand with a variable proportion (up to 60%) of fine to medium gravel predominates. In most cases, it is greater than or practically equal to the samples collected at +1.0 m MSL (foreshore) (Fig. 5).

Regarding the mineralogy, the beachrocks are almost exclusively composed of siliciclasts derived from granitoids (quartz, feldspar and biotite) (Table 4, Fig. 5). Excluding CA1, quartz is the dominant component (mean 71.8%), followed by felsic plutonic rock fragments (mean 14.7%) and feldspar (mean 11.0%). The lithology and granulometry (very fine to medium gravel) of the sediments result from the fact that they originated from the erosion of arenaceous mantles (grus) formed by the weathering of magmatic plutonic rocks. Those rock particles with a coarse or larger gravel size correspond to fragments of unaltered granitoids (granites and granodiorites) and hypabyssal rocks (mainly, granite porphyry, aplite and lamprophyre). CA2, 3, 4, 13 and 17 include fragments of rocks from thermal metamorphism (i.e. biotite and cordierite hornfels) in a maximum proportion of 1%. The petrological composition of the CA1 clasts is different from the rest: 55.2% schist, 8.1% quartz and 2.3% granite siliciclasts, but up to 34.2% of fragments of calcite and dolomite marble (Fig. 5). The lithological composition of the current beaches matches the composition of the adjacent beachrocks, reflecting that the sediments had the same origin (Table 4, Fig 5).

The bioclasts content in the studied beachrock samples was less than 1% of the total volume (mean 0.23%), except in one sample from CA6 (8.5%) (Table 2). Most of these bioclasts were medium sand size

Table 2. – Petrological characteristics of the beachrocks: particle size (VFG, very fine gravel (2-4 mm); FG, fine gravel (4-8 mm); MG, medium gravel (8-16 mm); CG, coarse gravel (16-31 mm); VCG, very coarse gravel (32-64 mm); Co, cobble (64-256 mm)); lithology (SIR, siliceous igneous rocks; SMR, siliceous metamorphic rocks; CMR, calcareous metamorphic rocks); Bioclasts (volume percentage with respect to total clast content); carbonates (weight percentage with respect to total rock, bioclasts included); Cement mineralogy of selected samples subjected to XRD and EDX microanalysis (ARG, aragonite; HMC, high magnesium calcite; LMC, low magnesium calcite).

Code	Particle size	Lithology	Bioclasts (%)	Carbonates (%)	Cement mineralogy
CA1	FG to Co	SMR-CMR	0.2	47.3	-
CA2	VFG to MG	SIR	0.1	10.4	-
CA3	VFG to MG	SIR	0.5-0.7	9.8-12.7	HMC
CA4	VFG to FG	SIR	0.2	11.6	-
CA5	VFG to FG	SIR	0.1	12.3	-
CA6	VFG to FG	SIR	0.3-8.5	12.5-22.7	HMC/LMC
CA7	VFG to FG	SIR	0.1	12.8-16.9	HMC
CA8	VFG to FG	SIR	0.1	18.2	HMC
CA9	VFG to FG	SIR	0.2	12.1	-
CA10	VFG to MG	SIR	0.2	13.3	HMC
CA11	VFG to MG	SIR	0.3	14.9	ARG/HMC
CA12	VFG to FG	SIR	0.1	10.8	HMC
CA13	VFG to FG	SIR	0.2	11.2	-
CA14	VFG to FG	SIR	0.8	9.1	HMC
CA15	VFG to Co	SIR	0.2	9.6-14.1	-
CA16	VFG to FG	SIR	0.1	15.5	ARG/HMC
CA17	VFG to MG	SIR	0.3	12.7	-
CA18	VFG to MG	SIR	0.1	13.3	-
CA19	VFG to FG	SIR	0.2	11.9	-

Table 3. – Grain size percentage of samples from study sites: Br, beachrock; Fo, current foreshore; Sh, current upper shoreface.

Opening diameter (mm)		8	4	2	1	0.5	0.25
		>FG	FG	VFG		Sand	
CA1	Br	35.6	33.5	20.4	8.0	2.5	0.0
	Fo	15.7	29.1	38.1	17.0	0.1	0.0
	Sh	0.8	6.4	23.7	54.4	14.0	0.7
CA2	Br	11.2	18.4	58.3	8.7	1.4	2.0
	Fo	7.3	8.8	83.4	0.5	0.0	0.0
	Sh	0.0	0.3	14.4	43.5	22.9	18.9
CA3	Br	11.2	24.5	36.9	14.1	13.3	0.0
	Fo	4.0	10.0	51.5	30.0	4.5	0.0
	Sh	0.0	0.0	0.0	3.2	26.8	70.0
CA4	Br	8.2	47.7	34.5	2.4	2.0	5.2
	Fo	4.8	21.9	71.0	1.9	0.4	0.0
	Sh	0.0	1.3	34.9	46.6	11.3	5.9
CA5	Br	5.3	25.0	61.6	4.4	1	2.7
	Fo	2.5	32.4	65.1	0.0	0.0	0.0
	Sh	0.0	1.3	50.9	47.2	0.6	0.0
CA6	Br	4.6	23.6	37.2	19.0	15.3	0.3
	Fo	2.2	15.3	45.5	21.2	14.1	1.7
	Sh	0.0	0.0	7.3	74.6	12.2	5.9
CA7	Br	6.1	15.9	49.4	23.2	5.4	0.0
	Fo	0.0	0.0	33.0	60.5	5.5	1.0
	Sh	0.0	0.0	0.0	0.3	3.7	96.0
CA8	Br	0.0	22.4	63.4	13.1	1.1	0.0
	Fo	0.0	11.2	84.9	3.4	0.5	0.0
	Sh	0.0	1.0	38.0	53.2	4.5	3.3
CA9	Br	1.5	4.7	45.3	28.4	14.7	5.4
	Fo	0.0	2.1	36.9	33.8	12.2	15.0
	Sh	0.0	11.0	10.7	17.4	32.6	28.3
CA10	Br	11.7	28.3	52.4	6.2	1.4	0.0
	Fo	10.0	16.0	72.5	1.5	0.0	0.0
	Sh	0.0	1.0	10.4	69.1	13.9	5.6
CA11	Br	17.6	41.3	30.3	9.6	1.2	0.0
	Fo	3.0	25.2	55.5	13.3	1.5	1.5
	Sh	0.0	0.0	33.8	62.7	1.1	2.4
CA12	Br	1.4	26.4	68.9	2.7	0.6	0.0
	Fo	1.8	19.3	70.8	8.0	0.1	0.0
	Sh	0.2	1.8	31.0	58.7	6.0	2.3
CA13	Br	3.6	28.0	59.5	5.8	1.3	1.8
	Fo	0.0	2.8	56.3	29.1	11.8	0.0
	Sh	0.0	0.8	19.0	33.4	38.9	7.9
CA14	Br	2.0	34.6	45.6	11.7	6.1	0.0
	Fo	0.0	0.0	59.8	34.6	5.1	0.5
	Sh	0.0	0.0	2.0	51.2	41.3	5.5
CA15	Br	13.4	42.1	22.8	15.2	6.3	0.2
	Fo	1.5	21.0	15.6	51.2	10.3	0.4
	Sh	0.0	0.0	1.3	65.4	32.3	1.0
CA16	Br	4.4	12.6	56.2	17.3	9.5	0.0
	Fo	3.7	5.2	62.5	27.1	1.5	0.0
	Sh	0.8	4.5	51.7	38.0	3.5	1.5
CA17	Br	27.1	17.6	30.1	17.5	3.8	3.9
	Fo	15.1	18.6	65.1	1.2	0.0	0.0
	Sh	0.0	2.8	3.1	13.6	71.1	9.4
CA18	Br	15.6	22.8	39.8	14.5	5.9	1.4
	Fo	8.9	11.0	56.1	17.8	6.2	0.0
	Sh	4.3	12.4	39.7	27.9	14.6	1.1
CA19	Br	1.5	29.4	54.1	12.7	2.3	0.0
	Fo	0.0	1.7	67.3	18.1	9.8	3.1
	Sh	0.0	0.6	20.1	32.7	37.9	8.7

Table 4. – Lithological composition (percentage of grains) of samples from study sites: Br, beachrock; Fo, current foreshore; Sh, current upper shoreface. CMR, calcareous metamorphic rocks (Cal: calcite and dolomite marble); SMR, siliceous metamorphic rocks (Sch: schist and hornfel); SIR, siliceous igneous rocks (Gra: granite, granodiorite, granite porphyry, aplite and lamprophyre; Qzt, quartz; Fdp, feldspar; Bit, biotite); Bio, bioclasts.

Lithology		Cal CMR	Sch SMR	Gra	Qzt SIR	Fdp	Bit	Bio
CA1	Br	34.2	55.2	2.3	8.1	0.0	0.0	0.2
	Fo	31.4	57.8	4.6	5.3	0.0	0.0	0.9
	Sh	32.0	53.8	5.8	5.6	0.0	0.0	2.8
CA2	Br	0.0	1.1	17.9	70.2	9.6	1.1	0.1
	Fo	0.0	1.7	25.9	63.1	7.3	1.7	0.3
	Sh	0.0	2.6	2.3	88.3	4.7	1.8	0.3
CA3	Br	0.0	0.1	24.9	61.2	8.9	4.3	0.6
	Fo	0.0	0.0	17.6	65.7	12.5	3.7	0.5
	Sh	0.0	0.2	3.1	64.7	19.6	5.8	6.6
CA4	Br	0.0	0.1	9.7	75.4	10.7	3.9	0.2
	Fo	0.0	0.7	13.2	72.2	13.2	0.7	0.0
	Sh	0.0	0.4	4.3	84.7	8.5	1.3	0.8
CA5	Br	0.0	0.0	14.8	42.3	12.2	0.6	0.1
	Fo	0.0	0.0	18.7	69.2	9.1	2.5	0.5
	Sh	0.0	0.0	4.3	79.9	11.0	3.8	1.0
CA6	Br	0.0	0.0	3.2	83.2	11.8	1.5	0.3 (8.5)
	Fo	0.0	0.0	2.3	79.4	15.6	1.9	0.8
	Sh	0.0	0.0	4.7	70.5	21.2	0.9	2.7
CA7	Br	0.0	0.0	13.4	68.2	16.3	2.0	0.1
	Fo	0.0	0.0	8.7	66.9	24.2	0.1	0.1
	Sh	0.0	0.0	2.1	71.3	18.4	4.6	3.6
CA8	Br	0.0	0.0	13.6	76.8	9.3	0.2	0.1
	Fo	0.0	0.0	4.8	78.1	16.4	0.5	0.2
	Sh	0.0	0.0	2.3	77.4	16.9	1.8	1.6
CA9	Br	0.0	0.0	9.5	75.7	12.2	2.4	0.2
	Fo	0.0	0.0	13.3	76.3	8.7	1.2	0.5
	Sh	0.0	0.0	4.6	81.2	7.9	5.0	1.3
CA10	Br	0.0	0.0	14.2	72.3	11.2	2.1	0.2
	Fo	0.0	0.0	7.8	80.6	8.4	1.6	1.6
	Sh	0.0	0.0	4.8	73.1	14.2	3.6	4.3
CA11	Br	0.0	0.0	11.3	78.2	8.5	1.7	0.3
	Fo	0.0	0.0	5.6	85.1	7.7	0.5	1.1
	Sh	0.0	0.0	0.6	82.0	11.5	2.6	3.3
CA12	Br	0.0	0.0	4.8	77.9	12.4	4.8	0.1
	Fo	0.0	0.0	3.7	81.7	14.1	0.3	0.2
	Sh	0.0	0.0	5.0	83.1	8.3	0.5	3.1
CA13	Br	0.0	0.2	6.4	74.0	13.6	5.6	0.2
	Fo	0.0	0.4	4.2	78.8	12.7	3.8	0.1
	Sh	0.0	0.6	1.3	77.4	13.2	7.1	0.4
CA14	Br	0.0	0.0	7.6	78.2	11.6	1.8	0.8
	Fo	0.0	0.0	2.2	76.4	15.8	4.4	1.2
	Sh	0.0	0.0	0.4	77.3	14.2	0.7	7.4
CA15	Br	0.0	0.0	44.2	51.9	3.7	0.0	0.2
	Fo	0.0	0.0	25.4	66.2	4.2	2.1	2.1
	Sh	0.0	0.0	10.5	63.9	14.2	8.2	3.2
CA16	Br	0.0	0.0	29.5	59.1	11.4	0.0	0.1
	Fo	0.0	0.0	5.7	70.6	20.2	0.0	3.5
	Sh	0.0	0.0	2.6	65.1	23.6	0.7	8.0
CA17	Br	0.0	0.7	12.9	73.0	12.7	0.4	0.3
	Fo	0.0	1.0	20.1	66.3	12.1	0.0	0.5
	Sh	0.0	0.4	0.4	85.3	11.3	2.2	0.4
CA18	Br	0.0	0.0	20.1	67.4	10.3	2.1	0.1
	Fo	0.0	0.0	17.5	65.0	13.9	3.6	0.0
	Sh	0.0	0.0	3.0	79.8	12.1	4.8	0.3
CA19	Br	0.0	0.0	7.2	78.2	12.0	2.4	0.2
	Fo	0.0	0.0	6.1	74.8	15.8	3.2	0.1
	Sh	0.0	0.0	2.3	80.3	12.1	4.8	0.5

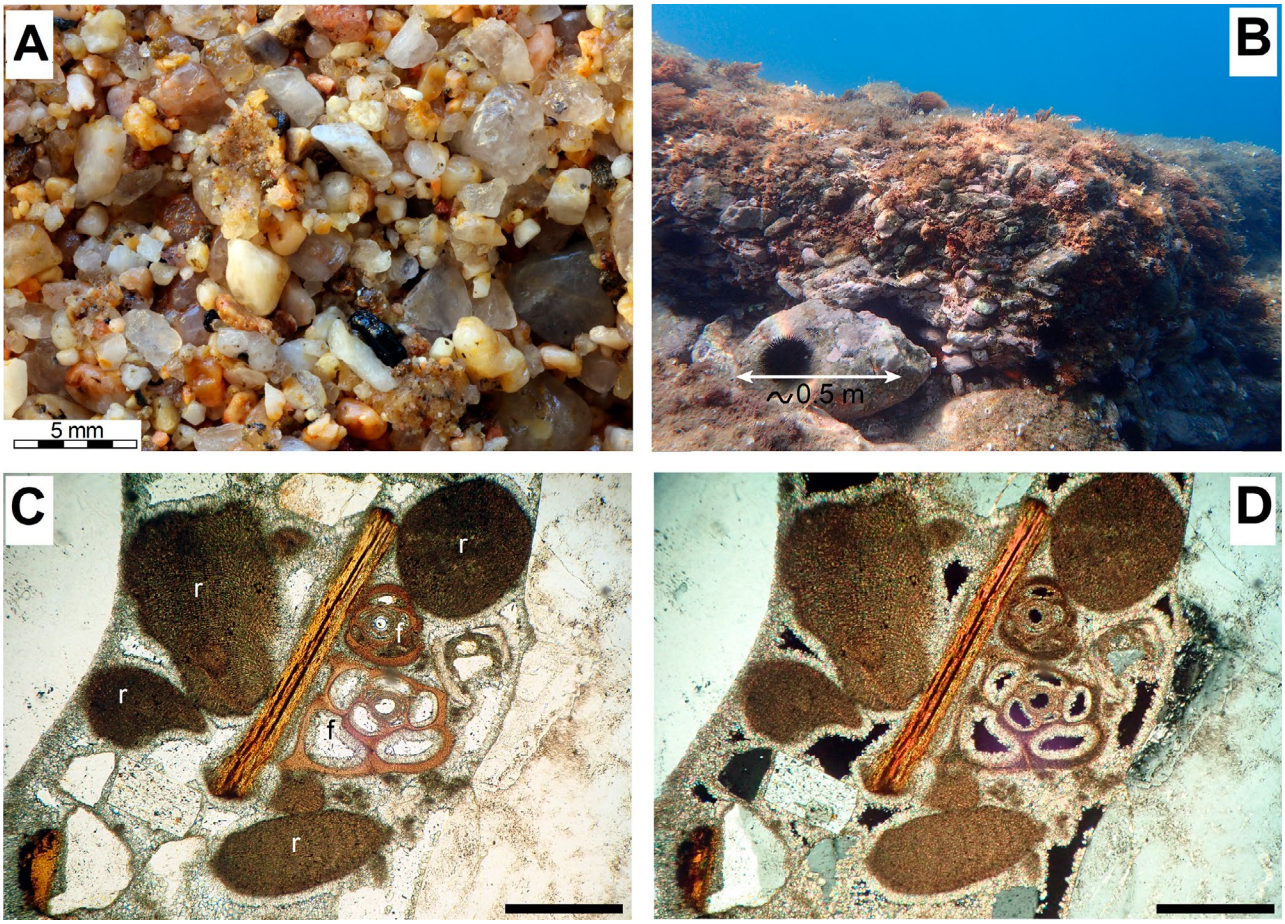

Fig. 6. – Petrological features. A, close-up image of a typical beachrock sample from the study area, constituted by very fine to medium gravel with a very coarse sand matrix (CA3). B, cemented very coarse gravels with rounded boulders at the base of the deposit (CA1). C, Thin section micrographs from the CA6 beachrock sample: f, foraminifera; r, coralline algae (left, plane polarized light; right, cross polarized light. Scale bar 0.25 mm).

(0.25 to 0.5 mm) and corresponded to Rhodophyta (algae) and Foraminifera (Fig. 6C), and to a lesser extent fragments of marine invertebrates (mainly bivalves, gastropods, echinoderms and Bryozoa). Exceptionally (up to 0.04% of the total volume), size seashells of bivalves larger than 2 mm (*Spondylus gaederopus*, *Pseudochama gryphina*, *Glycymeris* sp., *Barbatia barbata*, *Lima lima*, *Acanthocardia aculeata*) and gastropods (*Cerithium vulgatum*, *Patella ulyssiponensis*, *Hexaplex trunculus*, *Vermetus triquetrus*, *Conus ventricosus mediterraneus*, *Columbella rustica*, *Phorcus turbinatus* and *Stramonita haemastoma*) were observed, with variable attrition rates. All the reported species corresponded to fauna that currently inhabits the area.

The bioclast content of the current sediment collected in the foreshore was in all cases less than 5% of the total volume (mean 0.75%), and the presence of seashells larger than 2 mm was rare (up to 0.1%). Sediment samples from the upper shoreface contained a higher bioclast content (mean 2.72%), with a predominance of medium and coarse sand, but seashells larger than 2 mm were not uncommon (up to 0.5%).

The total carbonate content of the beachrock samples (i.e. percentage by weight of cement and bioclasts with respect to the total rock) ranged between 9.1% (CA14) and 18.2% (CA8), with a maximum of 22.7% corresponding to the sample richest in bioclasts from CA6 (Table 2). CA1 reached 47.3% due to its content in marble fragments.

The compositional analysis of the carbonates by XRD shows the generalized presence of high magnesium calcite (HMC), and also aragonite (ARG) only for the CA11 and CA16 samples (Table 2). Observation of samples by SEM showed that HMC formed an isopachous cement partially filling the pores, formed by steep or acute rhombohedral crystals 5 to 15 microns in size, arranged directly on the surface of the sediment particles (Fig. 7A, B). Occasionally they were partially covered by micrite, consisting of aggregates of acute rhombohedral crystals or anhedral grains (Fig. 7C). Low magnesium calcite (LMC) was also detected in the most proximal and emerged part of CA6 (0.85wt% Mg), formed by steep rhombohedral crystals ranging from 75 to 100 microns (Fig. 7D). ARG crystals were not observed in the cement samples under SEM.

Erosional features

When exposed, beachrocks are subject to the erosive action of waves, and consequently they are progressively degraded. Remnants of partially destroyed

Table 5. – Chronology. Code of laboratory: UAB, Tritium and Carbon-14 Dating Service of the Universitat Autònoma de Barcelona; POZ, Poznan Radiocarbon Laboratory; Beta, Beta Analytic; LDLUA, Luminescence Dating Laboratory of the University of A Coruña.

Beachrock and sample code	Laboratory code and dating method	Material	Radiocarbon age (yr BP)	OSL age (yr)	Calibrated age (yr)	Median probability date (yr)
CA1 PF1	UAB-E-121 Radiocarbon	*Patella ulyssiponensis*	1127±48		1071-1454 AD	1283 AD
CA1 PF2	Beta-590458 Radiocarbon	*Patella ulyssiponensis*	570±30		1598-post 1950 AD	1779 AD
CA3 LLA1	POZ-64042 Radiocarbon	*Pseudochama gryphina*	1170±50		1042-1427 AD	1243 AD
CA3 LLAW1	LDLUA OSL	Quartz		762±45	1207-1297 AD	1252 AD
CA6 CP1	Beta-590457 Radiocarbon	*Phorcus turbinatus.*	1510±30		693-1110 AD	906 AD
CA7 SAC1	Beta-590459 Radiocarbon	*Acanthocardia aculeata*	510±30		1665-post 1950 AD	1824 AD
CA11 BEL1	Beta-590460 Radiocarbon	*Stramonita haemastoma*	1030±30		1188-1529 AD	1365 AD
CA14 SP1	UAB-E-104 Radiocarbon	Coralline algae	2011±49		144-618 AD	386 AD
CA14 SP2	UAB-E-122 Radiocarbon	*Lima lima*	2171±50		59 BC-448 AD	198 AD
CA14 SP3	UAB-E-127 Radiocarbon	*Barbatia barbata*	938±49		1275-1644 AD	1439 AD
CA14 SP4	UAB-E-128 Radiocarbon	*Patella ulyssiponensis*	1000±48		1207-1586 AD	1387 AD
CA14 SP5	Beta-590461 Radiocarbon	*Stramonita haemastoma*	2400±30		343 BC-146 AD	85 BC
CA14 SP6	Beta-590462 Radiocarbon	*Acanthocardia aculeata*	630±30		1532-1939 AD	1724 AD
CA14 SPSW1	LDLUA OSL	Quartz		318±22	1674-1718 AD	1696 AD
CA17 MM1	Beta-5904 Radiocarbon	Charcoal	130±30		1673-1743 AD (28%) 1798-1942 AD (66%)	1834 AD
CA17 MM2	Beta-5904 Radiocarbon	*Patella* sp.	490±30		1679-1950 AD	1836 AD

beachrocks, consisting of grouped disaggregated blocks of sandstone and conglomerate up to 1 m^3 in size and located at depths of –3 m to –6 m MSL were identified near CA2, 4 and 10. They correspond to beachrocks that had been completely obliterated due to prolonged exposure.

Processes such as dissolution and bioerosion can also contribute to the degradation of beachrocks. Although dissolution has been reported as an important process in the development of erosional features in calcareous beachrocks (e.g. Hopley and Mackay 1978), in the deposits studied here, karstification is not a significant process because they have a siliceous composition and are submerged in the sea water. By contrast, the biological activity on the surface of all the studied beachrocks was great. Algae and other fouling organisms had degraded the surface, creating an altered coating layer, 0.5 mm to 15 mm thick, which was less competent than the fresh deposit due to its poorer cementation and higher organic matter content.

Nevertheless, the role of the biological processes in the degradation of these beachrocks is very limited when compared with the erosive effects of waves. These effects are (1) the undermining of the substrate on which they settle, (2) the differential erosion of beachrock layers, and (3) direct abrasion on the beachrock surface.

The undermining of the beachrock base was a generalized process in all studied cases, predominantly at the distal part that is more exposed to wave action. The bedrock (weathered granite and schist) is less resistant to erosion than the cemented beachrock. For this reason, the bedrock is eroded and the lower layers of the beachrock form visors. This process is more intense in CA7, where the substrate is built of unconsolidated marine sediments. In CA3, 7, 13, 14, 17 and 18, the undermining has generated subvertical fractures with rectilinear trends, spaced 0.5 to 5 m, which in plan view tend to form orthogonal systems, with one of the fracturing families parallel to the maximum length and the other to the width of the deposit (Fig. 8A). This is a common pattern in beachrocks reported in the literature (e.g. Strasser and Davaud 1986, Vousdoukas et al. 2007). Tilting and collapse of blocks dissected by the fracture system contribute to beachrock degradation. This process was reported by Caron (2012) to be enhanced during rough storms in tropical regions, but we have no data to corroborate whether it occurs analogously in the study area.

There is a stratigraphic control over the differential erosion of the layer sequence of all the studied beachrocks. Differential erosion generates metric-scale cuesta-type forms, with the steep side facing landwards

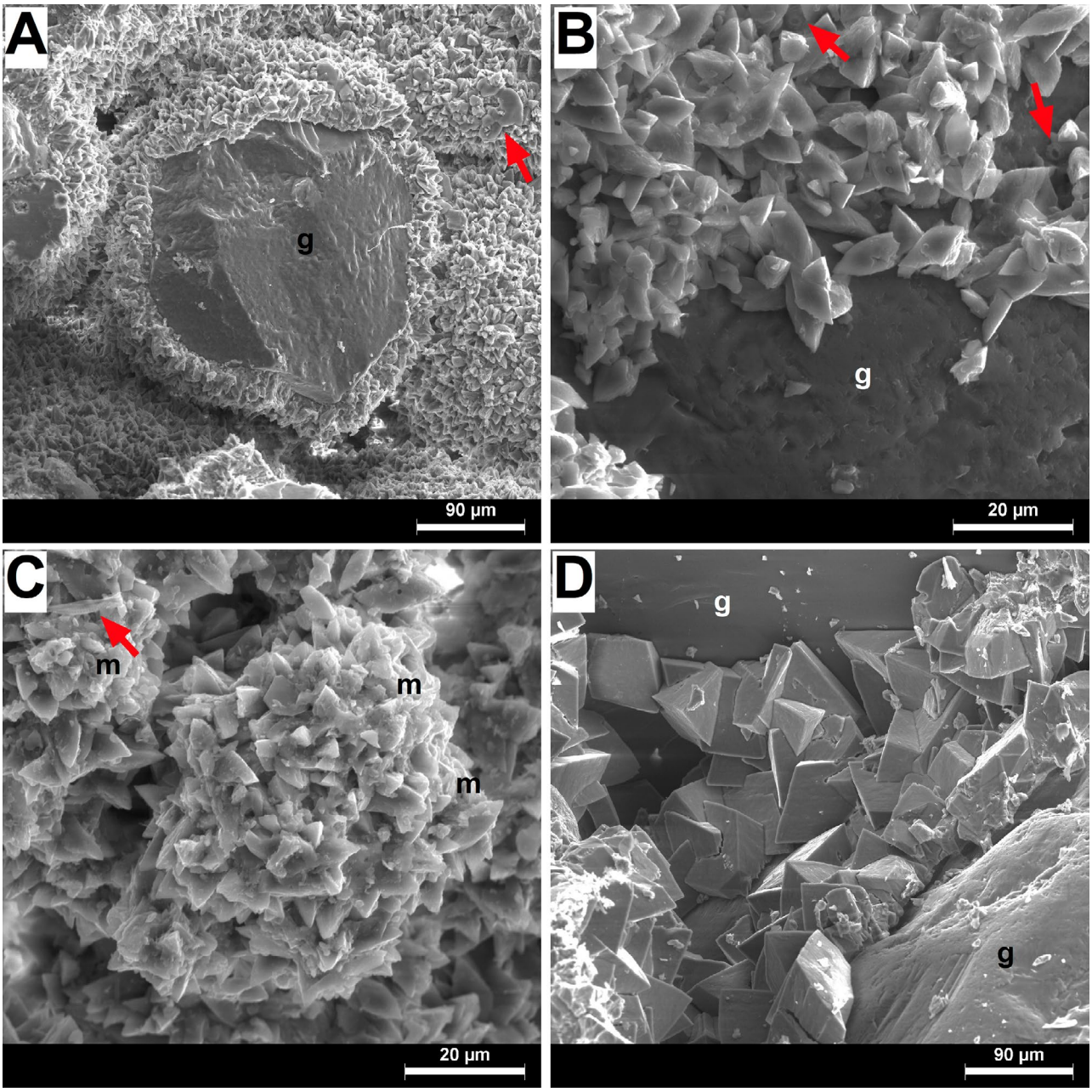

Fig. 7. – Scanning electron microscope (SEM) cements images. A, rhombohedral crystals of HMC cement forming rinds coating sedimentary grains (g), non-crystalline biogenic aggregates (red arrow) (CA11). B, acute rhombohedral crystals of HMC on sedimentary grains (g), coccoliths (red arrows) (CA3). C, rhombohedral crystals of HMC cement partially covered by scattered micrite aggregates (m), diatom frustule (red arrow) (CA7). D, steep rhombohedral crystals (spar) of LMC cement on sedimentary grains (g) (CA6).

(Fig. 8B). These landforms have been widely reported in the literature (e.g. Danjo and Kawasaki 2014). In the studied beachrocks, rough differences in competence of the different layers generate visors (Fig. 8C), arches and short tunnels (Fig. 8D).

One of the most widespread surface erosional forms of beachrocks are rounded erosional potholes (e.g. Hopley and Mackay 1978). In all the studied beachrocks these landforms are present, with diameters ranging from 5 to 250 cm and depths of up to 50 cm (Fig. 8E). They are often filled with gravels and cobbles. Their genesis is analogous to those formed in the rocky riverbeds. The progressive enlargement of both diameter and depth is most likely the result of cavitation and abrasion caused by gravels that are trapped inside the cavity and that violently twist and impact against the walls and bottom of the potholes during storms. The enlargement of the potholes favours interference and merging with each other, leading to more complex and irregular forms (Fig. 8F). The merging of hollows may evolve to sinuous rills, which act as flow paths for sediments during wave surges. In CA3, 4, 7, 9, 13 and 14, the bottoms of some erosional potholes are partially filled with cemented gravels. The cement is usually calcium carbonate, and occasionally metal oxides. The latter derive from the alteration of artificial

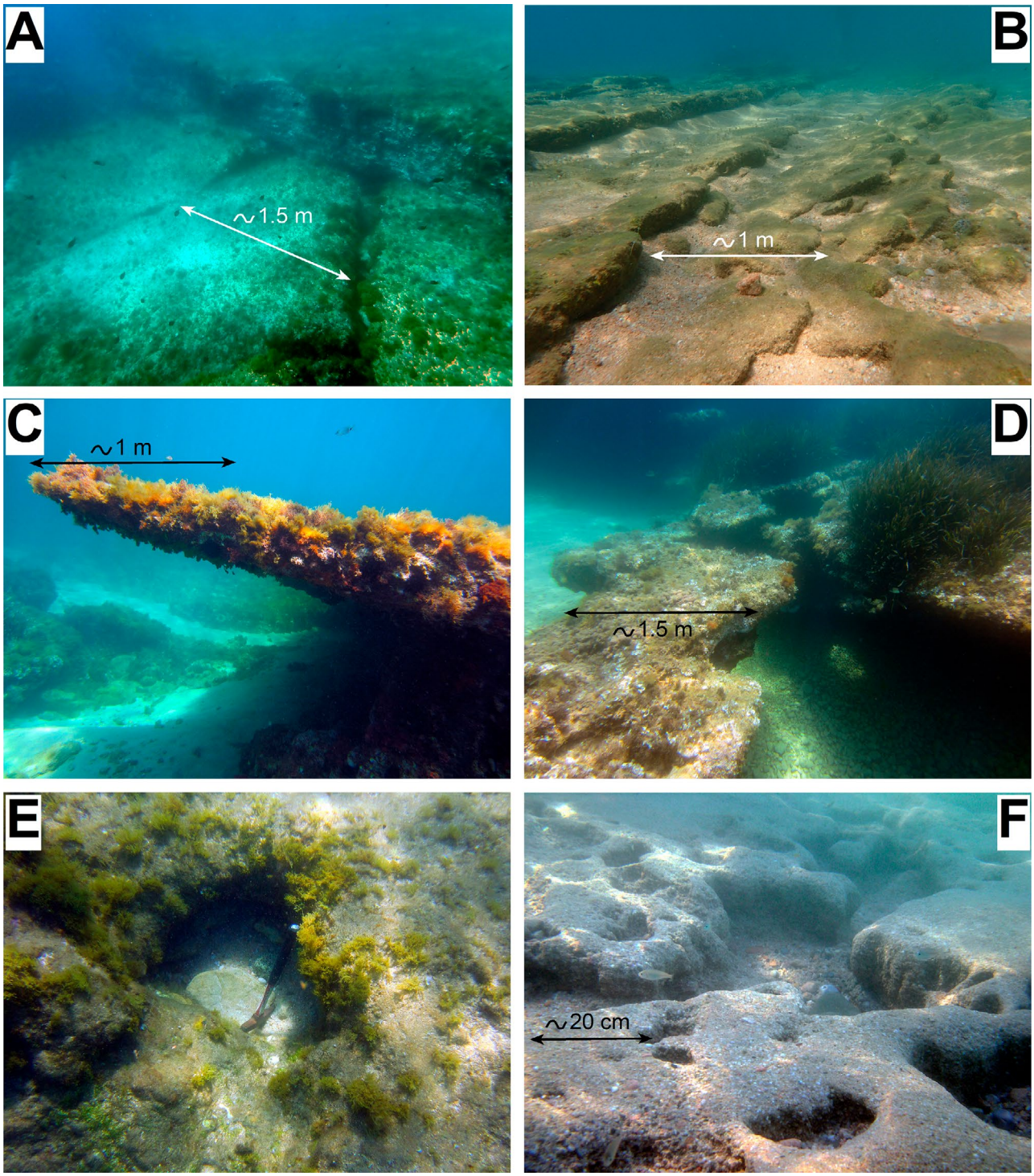

Fig. 8. – Erosion features. A, orthogonal joints delimiting partially collapsed blocks in the distal part of the CA17 beachrock. B, cuesta shape (CA14). C, visor (CA6). D, short tunnel partially collapsed (CA15). E, erosional potholes (CA9, hammer for scale). F, complex shapes caused by the growth and interference of erosional potholes (CA2).

iron artefacts and coins (copper and bronze), which, together with lead fishing weights, become trapped at the bottom of the cavity due to their high density.

Geochronology

Absolute ^{14}C ages from seven different beachrocks were determined by dating up to 12 carbonate seashells and 1 charcoal sample. The results obtained correspond to *terminus post quem* ages for the sediment cementing process, because shells and charcoals included in the beachrock sediments predate this process. A calcareous coralline algae bioconstructed level, emplaced between two overlapping levels in CA14, was also dated by ^{14}C. These algae were embedded on the lower level, which was necessarily already cemented. Later, the upper lev-

el was deposited and cemented on its top. All the obtained ages are from the Late Holocene (Table 5).

The complete geochronology of the sequence of two beachrocks that overlap on CA14 was established from six dates by ^{14}C (Fig. 4). The upper level (–0.25 to –2.5 m MSL deep) was dated between the 13th and 20th centuries AD (SP4, 1207-1586 cal AD; SP3, 1275-1644 cal AD; SP6, 1532-1939 cal AD). A significantly older age was reported for the lower level samples (mH= –3.75 m MSL) (SP5, 343 cal BC-146 cal AD; SP2, 59 cal BC-448 cal AD). In agreement with the intermediate stratigraphic position, the age of the embedded coralline algae level (SP1, 144-618 cal AD) is between those of the upper and lower levels.

The ^{14}C ages of two seashells from the upper level of CA1 (–1.0 to –2.5 m MSL deep, unit "a" in Fig. 3B) are similar to those of the upper level of CA14, ranging from the 11th to the 20th centuries AD (PF1, 1071-1454 cal AD; PF2, 1598-Post 1950 cal AD). The upper level of CA17 (–2.0 to –3.0 m MSL) also yielded a similar age (MM1, 1673-1743 AD (28%), 1798-1942 AD (66%); MM2, 1679-1950 AD).

The dating results of seashells from shallower beachrocks also falls within the same age range: CA3 (LLA1, 1042-1427 cal AD), CA7 (SAC1, 1665-post 1950 cal AD) and CA11 (BEL1, 1188-1529 cal AD), while CA6 sample is older (CP1, 693-1110 cal AD).

The upper level of CA14 was also dated by OSL (SPSW1, 1674-1718 AD), and the OSL date falls within the same time span as that obtained by ^{14}C. CA3 was also dated by OSL (LLAW1, 1207-1297 AD). The CA3 rock block sample was dated by both OSL and ^{14}C. The

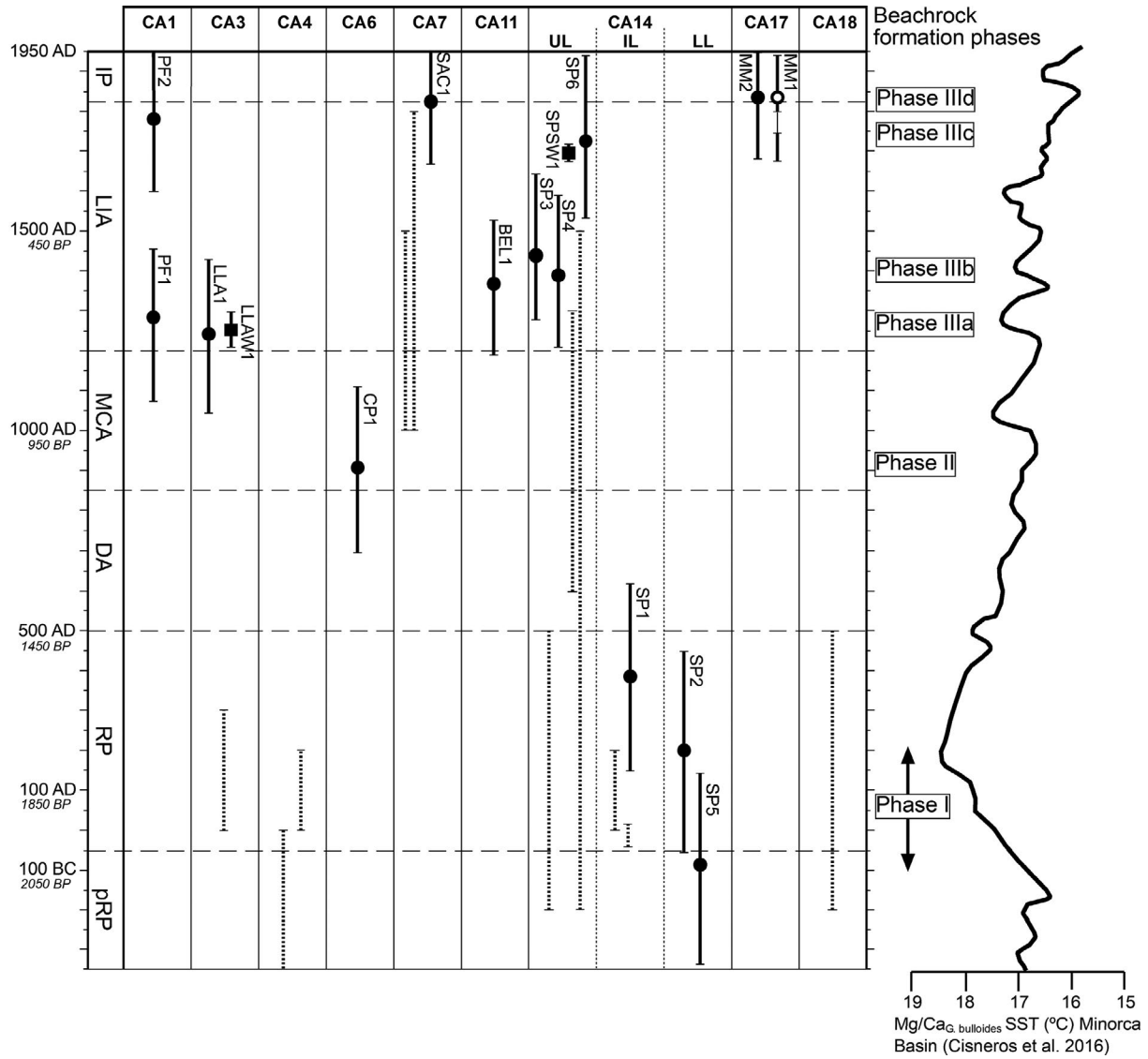

Fig. 9. – Chronology of beachrocks based on ^{14}C and OSL ages and formation phases for the study area. The time span for each sample is plotted. Black circles, median probability date for ^{14}C seashells. White circles, median probability date for ^{14}C charcoals. Black squares, median probability date for OSL samples. Black dotted lines, time span for anthropic remains. Climatic periods: pRP, pre-Roman Period; RP, Roman Period; DA, Dark Age; MCA, Medieval Climate Anomaly; LIA, Little Ice Age; IP, Industrial Period (Date intervals after Margaritelli et al. 2018). SST variation derived from $Mg/Ca_{G.\ bulloides}$ after Cisneros et al. (2016).

calibrated ^{14}C age (1042-1427 cal AD) is in agreement with the OSL date, and constrains the formation of this beachrock to around the 13th century AD, because the OSL age cannot be earlier than the age of the seashell.

Absolute ages were complemented by studying anthropic materials embedded in five of the beachrocks (Table 6). As bioclasts and charcoal, these artifacts establish a relative *terminus post quem* age for the cementation of the deposit. These artifacts are mostly worn fragments of tegulae, amphorae and pottery from the Roman Period (2nd c BC-5th c AD) (CA3, 14 and 18), although ceramic material from the Iberian period (6th c-1st c BC) (CA4) and from the Middle Ages to modern times (11th-18th c AD) was also identified with certainty (CA7 and 14). The overall results confirm the Late Holocene age of the studied beachrocks, which is consistent with the absolute ^{14}C and OSL ages. The upper level of CA14 (Fig. 4, Table 6, samples SPS1-9) yielded eight roughly worn ceramic shards and one glass fragment. Their ages span from Roman to medieval times (2nd c BC-15th c AD). The medieval artefacts (7th-15th c AD) are the ones that would be closest to the cementing date, since they are the youngest. Four ceramic fragments from Roman times were recovered from the intermediate level of CA14 (bioconstructed level of coralline algae, samples SPI1-4), whose chronology ranges from the 1st c BC to the 2nd c AD. Among all the elements, an amphora rim of the Tarraconense-1 type (sample SPI4) produced from 40 BC to 5 AD stands out (Tremoleda 2000).

DISCUSSION

Beach zone of carbonate cementation

It is widely accepted that, with some exceptions, the cementation of the beachrocks occurs in the intertidal beach zone (Webb et al. 1999, Vousdoukas et al. 2007) and that it is a consequence of the chemical and biological processes that take place there. On the studied coast, the astronomic tidal range is *ca*. 15 cm, so it lacks a proper intertidal zone.

Comparing the characteristics of the beachrock sediments and those of the foreshore and upper shoreface of the current beaches with the mineralogy of the beachrock cements allows us to establish that the cementation occurs in the swash zone and adjacent foreshore. This finding is well supported: First, the proportion of bioclasts determined in the samples rules out the possibility that the upper shoreface is part of the cemented sediments, because it contains a greater quantity of bioclasts (mean 2.72%) than the beachrocks (mean 0.23%). An exceptional sample from CA6 contains 8.5% of bioclasts, but its size is that of sand and it contains no shells larger than 2 mm. In contrast, the current shoreline sediment samples from this site contain up to 0.2% of seashells larger than 2 mm. The content (mean 0.75%) and size of the bioclasts in the sediment samples from the foreshore match better those of the beachrocks, suggesting that the cementing occurred in or near the emerged sector of the beach. Second, the grain size of the beachrocks is greater than that of the upper shoreface sediments of the current beaches (Fig. 5A, Table 3). Conversely, the current foreshore shows a particle size similar to that of the cemented deposits, but generally slightly finer. It should be noted that the CA3 and CA7 beaches have been subjected to nourishment with fine sand in recent years. However, this slight difference in grain size is also observed on beaches that have not been anthropically altered (for example CA1, 4 and 11). This suggests that the cementing could also affect sediments from the swash zone, which usually has a higher average particle size than the foreshore. Third, the beachrock cement (HMC) indicates that the precipitation occurred in contact with the seawater, which restricts the beachrock formation zone to the swash zone and adjacent foreshore. The ARG detected on two samples by XRD, which was not observed by SEM, may correspond to bioclasts. The presence of LMC in a sample from the most superficial part of CA6 (above the current sea level) indicates the local influence of meteoric water on the cementing processes.

Dating problems and calibration of the radiocarbon dates

Some limitations in the beachrocks formation ages obtained from dating seashells by ^{14}C should be considered. The post mortem residence time of seashells in the sediments of the beaches before their cementation is one of the longest. Long residence times imply that the dates obtained can be hundreds of years older than the cementation of the deposit (Mouslopoulou et al. 2015). In general, residence in carbonate environments is shorter than in siliciclastic environments due to greater bioerosion and dissolution (Kidwell et al. 2005). The seashell post mortem residence time in the study area is likely to be of the order of a few years to a few decades at most. Thus, by selecting for dating the seashells with little evidence of mechanical and biological erosion, it can be assumed that the ages obtained are close to the cementing time. This finding is well supported: First, the grain size of the deposits is dominated by gravel and the lithology by quartz, so the competence against mechanical erosion of the seashells during events of wave surges is presumably too low. Second, some of the studied beaches are very small (beach length <100 m in CA5, 8, 11, 12 and 15) (Table 1), and their uncemented sediments are almost completely washed after intense storms (e.g. CA4, 5 and 6 after the December 2008 and January 2020 storms). Third, in the cemented deposits and in the foreshore of the current beaches, the total bioclast content is very low (mean 0.23% and 0.75%, respectively) and the presence of seashells larger than 2 mm is exceptional (maximum of 0.04% and 0.1%, respectively), whereas in the current shoreface it is much higher (up to 0.5%). This suggests that the seashells are destroyed in the surf zone in a short time. Fourth, given the fragility of charcoal within a high-energy medium such as a beach, it can be assumed that its residence time is very low. The charcoal and shell dated at CA17, coming from the same rock block sample, show the same age, supporting the hypothesis that the residence time of the seashells is also low. Fifth, the

Table 6. – Chronology of archaeological remains. Code of laboratory: LAUdG, Archaeology Laboratory of the University of Girona; TM, Terracotta Museum.

Beachrock	Sample code	Laboratory	Material	Chronology
CA3	LLAF1	TM	Roman pottery	1st-3rd c AD
CA4	CAN1	LAUdG	Roman amphora	1st-2nd c AD
CA4	CAN2	LAUdG	Iberian pottery	6th-1st c BC
CA4	CAN3	TM	Roman amphora	1st-2nd c AD
CA7	SANC1	TM	Medieval pottery	11th-15th c AD
CA7	SANC2	TM	Medieval to Modern brick	11th-18th c AD
CA14	SPS1	LAUdG	Medieval coarse ware cooking-pot	7th-13th c AD
CA14	SPS2	LAUdG	Roman tegula	2nd c BC-5th c AD
CA14	SPS3	LAUdG	Roman tegula	2nd c BC-5th c AD
CA14	SPS4	LAUdG	Roman tegula	2nd c BC-5th c AD
CA14	SPS5	LAUdG	Roman tegula	2nd c BC-5th c AD
CA14	SPS6	LAUdG	Roman coarse ware cooking-pot	1st-2nd c AD
CA14	SPS7	LAUdG	Roman tegula	2nd c BC-5th c AD
CA14	SPS8	LAUdG	Roman tegula	2nd c BC-5th c AD
CA14	SPS9	LAUdG	Roman or Medieval glass bottle base	2nd c BC-15th c AD
CA14	SPI1	LAUdG	Roman coarse ware cooking-pot	1st-2nd c AD
CA14	SPI2	LAUdG	Roman amphora	1st-2nd c AD
CA14	SPI3	LAUdG	Roman coarse ware cooking-pot	1st-2nd c AD
CA14	SPI4	LAUdG	Roman amphora	40 yr BC-5 yr AD
CA18	CNY1	TM	Roman tegula	2nd c BC-5th c AD

time span for the ceramics embedded in the beachrocks is prior to the ^{14}C ages, which shows that the residence time of ceramic artefacts is longer than that of seashells. In addition, this also indicates that dating beachrocks only because of their archaeological remains may lead to overestimation of their real ages of formation.

Another limitation of ^{14}C dating is the incorporation of old carbon in the seashells (Mouslopoulou et al. 2015). Old carbon from substrate carbonates can accumulate in carbonate skeletons of marine organisms through ingestion. The only beachrock with calcareous rocks in the area is CA1, which includes 34.2% of marble lithoclasts (Fig. 5B, Table 4). The two ages obtained from the dating of this beachrock (1071-1454 cal AD and 1598-post 1950 cal AD) are the same as those obtained from the nearest and strictly siliciclastic ones (i.e. CA3, 1042-1427 cal AD; CA11, 1188-1529 cal AD; CA7, 1665-post 1950 cal AD), suggesting that the effect of old carbon is not significant here.

The main problem with the obtained ^{14}C ages is the calibration of the seashells due to the highly variability of the local reservoir effect of the sea (ΔR). The available values of ΔR applicable in the study area were reported by Siani et al. (2000) and are part of the Marine20 database. The eight nearest points (<400 km) have ΔR values that vary between –39±35 (Banyuls, at 6 km from the northern limit of the study area) and –255±35 (Toulon, *ca*. 230 km to the northeast). The weighted mean ΔR of these eight points is –140 ±74 yr.

The correspondence between the CA17's charcoal-calibrated age—which does not require ΔR correction—and the seashell extracted from the same rock block was used to adjust the applicable ΔR values. The charcoal has a median probability date (MPD) of 1834 cal AD and, applying the weighted mean ΔR of the eight nearest points in the seashell calibration, the MPD is 1836 cal AD. Therefore, the set ΔR value was considered suitable to calibrate all the ^{14}C ages of the seashells in the study area.

The OSL age of the rock block sample from CA3 beachrock further allowed us to test the consistency of the ΔR calibration value. Applying the nearest ΔR value (–39±35 yr), the MPD is 1338 cal AD. This age is younger than that obtained by OSL (1252 cal AD), which is not consistent, since the seashell must be either synchronous with or older than the burial date of the sediment in which it is included. Conversely, by applying the weighted mean ΔR of the eight nearest points (–140±74 yr), the MPD is 1243 cal AD, which in this case is consistent enough with the OSL results.

Phases of formation

Both the absolute dates (^{14}C, OSL) and the anthropic material dating indicate that the studied beachrocks are Late Holocene in age, corresponding to three main phases of formation (Fig. 9), from oldest to more modern:

Phase I is reported at the lower level (below -3.75 m MSL) of the beachrock CA14, with MPD ranging from 85 cal BC to 198 cal AD. These ages are consistent with that of the covering bioconstructed layer (MPD 386 cal AD), which formed after the lower level was cemented (Fig. 4). The lack of additional age data does not allow us to establish whether other beachrock levels located at similar depths (i.e. lower levels of CA1, CA16 and CA17) are contemporary, nor is possible to discern the age of the distant and deeper ledges that form the multiple-sequence beachrocks (i.e. CA6 and CA15).

Phase II is reported by the sample of the proximal and shallower level of the CA6 multiple-sequence beachrock (+0.25 m to –2.5 m MSL), with an MPD of 906 cal AD.

Phase III is reported in the upper levels (+0.5 m to –3.0 m) of CA1, 14 and 17 and in the CA3, 7 and 11. This phase comprises an MPD between 1243 and 1836 cal AD. All the shallowest and proximal beachrocks in the study area were probably formed during this phase. Specifically, the dates obtained for this phase are grouped into four sets: Phases IIIa, IIIb, IIIc and IIId. Samples PF1, LLA1 and LLAW1 belong to Phase IIIa, which chronologically comprises an MPD between 1243 and 1283 cal AD. Phase IIIb includes samples BEL1, SP3 and SP4, which have an MPD of between 1365 and 1439 cal AD. Phase IIIc includes samples PF2, SP6 and SPSW1, which have an MPD of between 1696 and 1779 cal AD. Phase IIId includes samples SAC1, MM1 and MM2, which have an MPD of between 1824 and 1836 cal AD (Fig. 9).

The palaeoclimatic context of beachrock formation phases

The SST is assumed to play a key role in the formation of beachrocks, because it controls the chemical reactions of calcium carbonate precipitation, evaporation and microbiological activity, which are favoured at higher temperatures (e.g. Morse and Mackenzie 1990, Zhao et al. 2019). Therefore, a correspondence between the phases of beachrock formation and warm climatic conditions would be expected. The SST variability during the last 2.7 kyr in the western Mediterranean was established from sediment cores recovered from the north of Minorca island (Fig. 1), from the $Mg/Ca_{G.\ bulloides}$ and alkenones ratios and from $\delta^{18}O$ measurements (i.e. Moreno et al. 2012, Cisneros et al. 2016, Margaritelli et al. 2018). This SST variability and the climate periods are represented in Figure 9. The MPD of samples corresponding to Phase I and the algal bioconstructed layer fall within the warm and humid Roman Period. It is noteworthy that Roman Period conditions are the warmest of the last 2 kyr (Margaritelli et al. 2020). Phase II corresponds to the warm and arid Medieval Climate Anomaly, which indicates that a dry climate also favours cementation by evaporation of the beach sediment porewater. Phase III covers the Little Ice Age and the Industrial Period. Specifically, Phase IIIa and Phase IIIb correspond to the early warmer Little Ice Age interval (LIAa, Cisneros et al. 2016). A fitted positive correlation between the age ranges of both phases and the SST variation is observed, illustrating that the SST rise promotes beachrock formation (Fig. 9). On the other hand, Phase IIIc does not fit the high SST condition, but the age range for Phase IIIc (MPD 1696-1779 cal AD) roughly matches the relative climate optimum recorded in Europe between 1715 and 1760 cal AD (Oliva et al. 2018). Furthermore, the arid pulse recorded at several sites of NE Spain between 1730 and 1790 cal AD (Corella et al. 2013) also matches Phase IIIc. Phase IIId (MPD 1824-1836 cal AD), dated within the Industrial Period, also does not correlate with high SST records. According to Oliva et al. (2018), the study area suffered extreme events between 1815 and 1835, including prolonged droughts. The instrumental precipitation records also reported a dry period between the 1810s and the 1840s, with more than 80% of the precipitation records below the average (Prohom et al. 2015). These data suggest that this beachrock formation phase may be related to severe porewater evaporation processes.

CONCLUSIONS

The ^{14}C and OSL absolute dates of rock block samples and seashells and the dating of remains of the embedded historical artifacts allowed us to differentiate three formation phases for the studied beachrocks, all belonging to Late Holocene: Phase I (MPD 85 cal BC-198 cal AD), the basal level of CA14 (below –3.75 m MSL), which falls within the warm and humid Roman Period; Phase II (MPD 906 cal AD), the proximal and shallower level of the CA6 multiple sequence (+0.25 m to –2.5 m MSL), which falls within the warm and arid Medieval Climate Anomaly; and Phase III, at the upper levels (+0.5 m to –3.0 m MSL) of CA1, 3, 7, 11, 14 and 17, which falls within the Little Ice Age and the Industrial Period. Phase III encompasses four correlative subphases. Phase IIIa (MPD 1243-1283 cal AD) and Phase IIIb (MPD 1365-1439 cal AD) fit with relatively high SST. Phase IIIc (MPD 1696-1779 cal AD) does not to fit high SST conditions but roughly coincides with the relative climate optimum recorded in Europe between 1715 and 1760 cal AD and with the arid pulse recorded at several sites of NE Spain between 1730 and 1790 cal AD. Phase IIId (MPD 1824-1836 cal AD) corresponds to the Industrial Period, and also does not fit high SST records, but could be related to extreme drought events between the 1810s and the 1840s.

The chronology of each recorded cementation phase shows a good temporal correspondence with warm and/or dry palaeoclimatic conditions, indicating that beachrocks in the study area are palaeoclimatic indicators. The cementation of the beach sediments occurs in the swash zone and adjacent foreshore, as a consequence of the precipitation of HMC in conditions of warm sea water favoured by episodes of drought.

ACKNOWLEDGEMENTS

The authors thank the anonymous reviewers and the editor for their constructive comments and suggestions, which greatly improved the quality of the paper. This research did not receive any specific funding from any public, commercial or not-for-profit funding agency.

REFERENCES

Arrieta N., Goienaga N., Martinez-Arkarazo I., et al. Beachrock formation in temperate coastlines: examples in sand-gravel beaches adjacent to the Nerbioi-Ibaizabal Estuary (Bilbao, Bay of Biscay, North of Spain). Spectrochim. Acta A 80: 55-65. https://doi.org/10.1016/j.saa.2011.01.031

Avcioglu M., Yigitbas E., Erginal A.E. 2016. Beachrock formation on the coast of Gökçeada island and its relation to the active tectonics of the region, northern Aegean Sea, Turkey. Quat. Int. 401: 141-152. https://doi.org/10.1016/j.quaint.2015.10.108

Bernier P., Guidi JB., Böttcher M.E. 1997. Coastal progradation and very early diagenesis of ultramafic sands as a result of

rubble discharge from asbestos excavations (northern Corsica, western Mediterranean). Mar. Geol. 144: 163-175. https://doi.org/10.1016/S0025-3227(97)00086-8
Bloch J.P., Trichet J. 1966. Un exemple de grès de plage (côte Ligure Italienne). Mar. Geol. 4: 373-377. https://doi.org/10.1016/0025-3227(66)90041-7
Caldas L.H.D.O., Stattegger K., Vital H. 2006. Holocene sea-level history: Evidence from coastal sediments of the northern Rio Grande do Norte coast, NE Brazil. Mar. Geol. 228: 39-53. https://doi.org/10.1016/j.margeo.2005.12.008
Calvet J., Gallart F. 1973. Esquema morfológico de la costa catalana. Acta Geol. Hisp. 4: 125-130
Calvet F., Cabrera M.C., Carracedo J.C., et al. 2003. Beachrocks from the island of La Palma (Canary Islands, Spain). Mar. Geol. 197: 75-93. https://doi.org/10.1016/S0025-3227(03)00090-2
Caron V. 2012. Geomorphic and sedimentologic evidence of extreme wave events recorded by beachrocks: A case study from the island of St. Bartholomew (Lesser Antilles). J. Coast. Res. 28: 811-828. https://doi.org/10.2112/JCOASTRES-D-10-00152.1
Casas-Prat M., Sierra J.P. 2012. Trend analysis of wave direction and associated impacts on the Catalan coast. Clim. Change 115: 667-691. https://doi.org/10.1007/s10584-012-0466-9
Cisneros M., Cacho I., Frigola J., et al. 2016. Sea surface temperature variability in the central-western Mediterranean Sea during the last 2700 years: a multi-proxy and multi-record approach. Clim. Past 12: 849-869. https://doi.org/10.5194/cp-12-849-2016
Corella J.P., Stefanova V., El Anjoumi A., et al. 2013. A 2500-year multi-proxy reconstruction of climate change and human activities in northern Spain: The Lake Arreo record. Palaeogeogr. Palaeoclimatol. Palaeoecol. 386: 555-568. https://doi.org/10.1016/j.palaeo.2013.06.022
Danjo T., Kawasaki S. 2014. Characteristics of beachrocks: A Review. Geotech. Geol. Eng. 32: 215-246. https://doi.org/10.1007/s10706-013-9712-9
Daryono L.R., Nakashima K., Kawasaki S., et al. 2020. Sediment characteristics of beachrock: A baseline investigation based on microbial induced carbonate precipitation at Krakal-Sadranan Beach, Yogyakarta, Indonesia. Appl. Sci. 10: 520. https://doi.org/10.3390/app10020520
El-Sayed M.K. 1988. Beachrock cementation in Alexandria, Egypt. Mar. Geol. 80: 29-35. https://doi.org/10.1016/0025-3227(88)90070-9
Erginal A.E., Erenoglu R.C., Yildirim C., et al. 2021. Co-seismic beachrock deformation of 8th century AD earthquake in middle strand of north Anatolian fault, lake Iznik, NW Turkey. Tectonophysics 799: 228690. https://doi.org/10.1016/j.tecto.2020.228690
Font Y., Calvet F. 1997. Beachrocks holocenos de la Isla de la Reunión, Océano Índico. Cuad. Geol. Iberica 22: 81-102.
Friedman G.M. 1998. Rapidity of marine carbonate cementation - implications for carbonate diagenesis and sequence stratigraphy: perspective. Sediment. Geol. 119: 1-4. https://doi.org/10.1016/S0037-0738(98)00075-X
Friedman G.M. 2011. Beachrocks record Holocene events, including natural disasters. Carbonates Evaporites 26: 97-109. https://doi.org/10.1007/s13146-011-0056-3
Furlani S., Pappalardo M., Gómez-Pujol L., Chelli A. 2014. The rock coast of the Mediterranean and Black seas. Geological Society, London, Memoirs 40: 89-123. https://doi.org/10.1144/M40.7
Gischler E. 1994. Sedimentation on three Caribbean atolls: Glovers Reef, Lighthouse Reef and Turneffe Islands. Facies 31: 243-254. https://doi.org/10.1007/BF02536941
Gómez J., Espino M., Sánchez-Arcilla A., et al. 2005: Extreme wave conditions in a torrential climate, The Catalan case. Ocean Wave Measurement and Analysis, Proceedings of the Fifth International Symposium WAVES, CD-ROM.
Holail H., Rashed M. 1992. Stable isotopic composition of carbonate-cemented recent beachrock along the Mediterranean and the Red Sea coasts of Egypt. Mar. Geol. 106: 141-148. https://doi.org/10.1016/0025-3227(92)90059-Q
Hopley D. 1986. Beachrock as a sea-level indicator. In: van de Plassche O. (ed), Sea-Level Research: A manual for the collection and evaluation of data. Geo Books, Regency House, Norwich, England, pp. 157-173. https://doi.org/10.1007/978-94-009-4215-8_6
Hopley D., MacKay M.G. 1978. An investigation of morphological zonation of beach rock erosional features. Earth Surf. Proc. Land. 3: 363-377. https://doi.org/10.1002/esp.3290030405
Kelletat D. 2006. Beachrock as sea-level indicator? Remarks from a geomorphological point of view. J. Coast. Res. 22: 1558-1564. https://doi.org/10.2112/04-0328.1
Kidwell S.M., Best M.M.R., Kaufman D. 2005. Taphonomic tradeoffs in tropical marine death assemblages: differential time-averaging, shell loss, and probable bias in siliciclastic versus carbonate facies. Geology 33: 729-732. https://doi.org/10.1130/G21607.1
Kneale D., Viles H.A. 2000. Beach cement: incipient $CaCO_3$-cemented beachrock development in the upper intertidal zone, North Uist, Scotland. Sediment. Geol. 132: 165-170. https://doi.org/10.1016/S0037-0738(00)00029-4
Longhitano S.G. 2015. Short-term assessment of retreating vs. advancing microtidal beaches based on the backshore/foreshore length ratio: Examples from the Basilicata Coasts (Southern Italy). Open J. Mar. Sci. 5: 123-145. https://doi.org/10.4236/ojms.2015.51011
Magaritz M., Gavish E., Bakler N., Kafri U. 1979. Carbon and oxygen isotope composition-indicators of cementation environment in Recent, Holocene, and Pleistocene sediments along the coast of Israel. J. Sediment. Petrol. 49: 401-412 https://doi.org/10.1306/212F7757-2B24-11D-7-8648000102C1865D
Margaritelli G., Cisneros M., Cacho I., et al. 2018. Climatic variability over the last 3000 years in the central - western Mediterranean Sea (Menorca Basin) detected by planktonic foraminifera and stable isotope records. Glob. Planet Change 169: 179-187. https://doi.org/10.1016/j.gloplacha.2018.07.012
Margaritelli G., Cacho I, Català A., et al. 2020. Persistent warm Mediterranean surface waters during the Roman period. Sci. Rep. 10: 10431. https://doi.org/10.1038/s41598-020-67281-2
Martín-Vide J. Raso J.M. 2008. Atles climàtic de Catalunya. Període 1961-1990. Termopluviometria, ICC and SMC, Barcelona, 32 pp.
Mauz B., Vacchi M., Green A., et al. 2015. Beachrock: A tool for reconstructing relative sea level in the far-field. Mar. Geol. 362: 1-16. https://doi.org/10.1016/j.margeo.2015.01.009
McCutcheon J., Nothdurft LD., Webb GE., et al. 2016. Beachrock formation via microbial dissolution and re-precipitation of carbonate minerals. Mar. Geol. 382: 122-135. https://doi.org/10.1016/j.margeo.2016.10.010
McCutcheon J., Nothdurft L.D., Webb G.E., et al. 2017. Building biogenic beachrock: Visualizing microbially-mediated carbonate cement precipitation using XFM and a strontium tracer. Chem. Geol. 465: 21-34. https://doi.org/10.1016/j.chemgeo.2017.05.019
Mendoza E.T., Jimenez J.A., Mateo J. 2011. A coastal storms intensity scale for the Catalan sea (NW Mediterranean). Nat. Hazards Earth Syst. Sci. 11: 2453-2462. https://doi.org/10.5194/nhess-11-2453-2011
Moissette P., Koskeridou E., Cornée J.J., André JP. 2013. Fossil assemblages associated with submerged beachrock beds as indicators of environmental changes in terrigenous sediments: Examples from the Gelasian (Early Pleistocene) of Rhodes, Greece. Palaeogeogr. Palaeoclimatol. Palaeoecol. 369: 14-27. https://doi.org/10.1016/j.palaeo.2012.09.007
Moreno A., Pérez A., Frigola J., et al. 2012. The Medieval Climate Anomaly in the Iberian Peninsula reconstructed from marine and lake records. Quat. Sci. Rev. 43: 16-32. https://doi.org/10.1016/j.quascirev.2012.04.007
Morse J.W., Mackenzie F.T. 1990. Geochemistry of sedimentary carbonates. Developments in Sedimentology, Vol. 48. Elsevier, Amsterdam, 707 pp.
Mouslopoulou V., Begg J., Nicol A., et al. 2015. Formation of Late Quaternary paleoshorelines in Crete, Eastern Mediterranean. Earth Planet. Sci. Lett. 431: 294-307. https://doi.org/10.1016/j.epsl.2015.09.007
Muhs D., Simmons KR., Meco J., Porat N. 2015. Uranium-series ages of fossil corals from Mallorca, Spain: The "Neotyrrhenian" high stand of the Mediterranean Sea revisited. Palaeogeogr. Palaeoclimatol. Palaeoecol. 438: 408-424. https://doi.org/10.1016/j.palaeo.2015.06.043

Neumeier U. 1998. Le rôle de l'activité microbienne dans la cimentation précoce des beachrocks (sédiments intertidaux), PhD thesis 2994, University of Geneva, 183 pp.
Oliva M., Ruiz-Fernández J., Barriendos M., et al. 2018. The Little Ice Age in Iberian mountains. Earth-Sci. Rev. 177: 175-208. https://doi.org/10.1016/j.earscirev.2017.11.010
Pagán J.I., Aragonés L., Tenza-Abril A.J., Pallarés P. 2016. The influence of anthropic actions on the evolution of an urban beach: Case study of Marineta Cassiana beach, Spain. Sci. Total Environ. 559: 242-255. https://doi.org/10.1016/j.scitotenv.2016.03.134
Pascual J. 2019. Estacions meteorològiques de l'Estartit i de Torroella de Montgrí, http://meteolestartit.cat/mar/nivell-del-mar/, accessed 2019-1-29.
Prohom M., Barriendos M., Sanchez-Lorenzo A. 2015. Reconstruction and homogenization of the longest instrumental precipitation series in the Iberian Peninsula (Barcelona, 1786-2014). Int. J. Climatol. 36: 3072-3087. https://doi.org/10.1002/joc.4537
Psomiadis D., Tsourlos P., Albanakis K. 2009. Electrical resistivity tomography mapping of beachrocks: application to the island of Thassos (N. Greece). Environ. Earth Sci. 59: 233-240. https://doi.org/10.1007/s12665-009-0021-9
Psomiadis D., Albanakis K., Zisi N., et al. 2014. Clastic sedimentary features of beachrocks and their palaeo-environmental significance: comparison of past and modern coastal regimes. Int. J. Sediment Res. 29: 260-268. https://doi.org/10.1016/S1001-6279(14)60041-X
Pullen D. 2013. The life and death of a Mycenaean port town: Kalamianos on the Saronic Gulf. J. Marit. Archaeol. 8: 245-262. https://doi.org/10.1007/s11457-013-9113-5
Ramachandran A.L., Polat P., Mukherjee A., Dhami N.K. 2020. Understanding and creating biocementing beachrocks via biostimulation of indigenous microbial communities. Appl. Microbiol. Biotechnol. 104: 3655-3673. https://doi.org/10.1007/s00253-020-10474-6
Rey D., Rubio B., Bernabeu A.M., Vilas F. 2004. Formation, exposure, and evolution of a high-latitude beachrock in the intertidal zone of the Corrubedo complex (Ria de Arousa, Galicia, NW Spain). Sediment. Geol. 169: 93-105. https://doi.org/10.1016/j.sedgeo.2004.05.001
Roqué C., Pallí L. 1995. Playas fósiles sumergidas en la Costa Brava meridional (Girona). In: Aleixandre T., Pérez-González A. (eds), Reconstrucción de paleoambientes y cambios climáticos durante el Cuaternario. Centro de Ciencias Medioambientales, CSIC, Madrid, pp. 15-25.
Roqué C., Pallí L. 1997. Ancient submerged beaches of the Costa Brava (Girona, Spain). Geogr. Fis. e Din. Quat.-Supplementi III, 1: 333-334.
Russell R.J. 1962. Origin of beach rock. Z. Geomorphol. 6: 1-16.
Russell R.J., McIntire WG. 1965. Southern hemisphere beach rock. Geogr. Rev. 55: 17-45. https://doi.org/10.2307/212853
Sánchez-Arcilla A., González-Marco D., Bolaños R. 2008. A review of wave climate and prediction along the Spanish Mediterranean coast. Nat Hazards Earth Syst. Sci. 8: 1217-1228. https://doi.org/10.5194/nhess-8-1217-2008
Sanchez-Vidal A., Canals M., Calafat AM., et al. 2012. Impacts on the deep-sea ecosystem by a severe coastal storm. PLoS ONE 7: e30395. https://doi.org/10.1371/journal.pone.0030395
Sanuy M., Rigo T., Jiménez J.A., Llasat M.C. 2020. Classifying compound coastal storm and heavy rainfall events in the north-western Spanish Mediterranean. Hydrol. Earth Syst. Sci. Discuss [preprint] https://doi.org/10.5194/hess-2020-560
Scoffin T.P., Stoddart D.R. 1987. Beachrock and intertidal cements. In: Scoffin TP. (ed), An introduction to carbonate sediments and rocks. Glasgow: Blackie Publishing Company, pp. 401-425.
Serrano E., Coma R., Ribes M., et al. 2013. Rapid northward spread of a zooxanthellate coral enhanced by artificial structures and sea warming in the Western Mediterranean. PLoS ONE 8(1): e52739. https://doi.org/10.1371/journal.pone.0052739
Siani G., Paterne M., Arnold M., et al. 2000. Radiocarbon reservoir ages in the Mediterranean Sea and Black Sea. Radiocarbon 42: 271-280. https://doi.org/10.1017/S0033822200059075
Stattegger K., Tjallingii R., Saito Y., et al. 2013. Mid to late Holocene sea-level reconstruction of Southeast Vietnam using beachrock and beach-ridge deposits. Glob. Planet Change 110: 214-222. https://doi.org/10.1016/j.gloplacha.2013.08.014
Strasser A., Davaud E. 1986. Formation of Holocene limestone sequences by progradation, cementation, and erosion: two examples from the Bahamas. J. Sediment. Petrol. 56: 422-428. https://doi.org/10.1306/212F8936-2B24-11D-7-8648000102C1865D
Strasser A., Davaud E., Jedoui Y. 1989. Carbonate cements in Holocene beachrock: example from Bahiret et Biban, southeastern Tunisia. Sediment. Geol. 62: 89-100. https://doi.org/10.1016/0037-0738(89)90103-6
Stuiver M., Reimer P.J., Reimer R.W. 2021. CALIB 8.2 [WWW program] at http://calib.org, accessed 2021-3-18.
Tremoleda J. 2000. Industria y artesanado cerámico de época romana en el nordeste de Cataluña (Época augústea y alto-imperial). BAR International Series 835, 341 pp.
Turner R.J. 2005. Beachrock. In Schwartz ML. (ed), Encyclopedia of Coastal Science. Klumer Academic Publishers, The Netherlands, pp. 183-186.
Vacchi M., Marriner N., Morhange C., et al. 2016. Multiproxy assessment of Holocene relative sea-level changes in the western Mediterranean: Sea-level variability and improvements in the definition of the isostatic signal. Earth Sci. Rev. 155: 172-197. https://doi.org/10.1016/j.earscirev.2016.02.002
Vieira M.M., Ros L.F. 2006. Cementation patterns and genetic implications of Holocene beachrocks from northeastern Brazil. Sediment. Geol. 192: 207-230. https://doi.org/10.1016/j.sedgeo.2006.04.011
Vousdoukas M.I., Velegrakis A.F., Plomaritis, T.A. 2007. Beachrock occurrence, characteristics, formation mechanisms and impacts. Earth Sci. Rev. 85: 23-46. https://doi.org/10.1016/j.earscirev.2007.07.002
Vousdoukas M.I., Velegrakis A.F., Karambas T.V. 2009. Morphology and sedimentology of a microtidal beach with beachrocks: Vatera, Lesbos, NE Mediterranean. Cont. Shelf Res. 29: 1937-1947. https://doi.org/10.1016/j.csr.2009.04.003
Webb G.E., Jell J.S., Baker J.C. 1999. Cryptic intertidal microbialites in beachrock, Heron Island, Great Barrier Reef: implications for the origin of microcrystalline beachrock cement. Sediment. Geol. 126: 317-334. https://doi.org/10.1016/S0037-0738(99)00047-0
Yaltirak C., Sakinç M., Aksu A.E., et al. 2002. Late Pleistocene uplift history along the southwestern Marmara Sea determined from raised coastal deposits and global sea-level variations. Mar. Geol. 190: 283-305. https://doi.org/10.1016/S0025-3227(02)00351-1
Zhao N., Shen D.S., Shen J.W. 2019. Formation mechanisms of beach rocks and its controlling factors in Coral Reef area, Qilian islets and cays, Xisha Islands, China. J. Earth Sci. 30: 728-738. https://doi.org/10.1007/s12583-018-0981-3